Mechanism of Torrential Rain Associated with the Mei-yu Development during SCSMEX-98

JIAN-HUA QIAN[1]

Mesoscale Atmospheric Processes Branch, Laboratory for Atmospheres
NASA/Goddard Space Flight Center, Greenbelt, Maryland
and Universities Space Research Association, Greenbelt, Maryland

WEI-KUO TAO

Mesoscale Atmospheric Processes Branch, Laboratory for Atmospheres
NASA/Goddard Space Flight Center, Greenbelt, Maryland

K.-M. LAU

Climate and Radiation Branch, Laboratory for Atmospheres
NASA/Goddard Space Flight Center, Greenbelt, Maryland

Submit to *Monthly Weather Review*

January 2002

[1] *Corresponding author address:* Dr. Jian-Hua (Joshua) Qian, International Research Institute for climate prediction, Lamont-Doherty Earth Observatory of Columbia University, 61 Route 9W, Palisades, NY 10964. email: jqian@iri.columbia.edu

ABSTRACT

A case of torrential precipitation process in the Mei-yu front, an Asian monsoon system east to the Tibetan Plateau, is studied with the coupled Penn State University/NCAR MM5 and NASA/GSFC PLACE (Parameterization for Land-Atmosphere-Cloud Exchange) models. Remote and local impacts of water vapor on the location and intensity of Mei-yu precipitation are studied by numerical experiments. Results demonstrate that the water vapor source for this heavy precipitation case in Yangtze river basin is derived mostly from the Bay of Bengal, transported by the southwesterly low-level jet (LLJ) southeast to the Tibetan Plateau. The moist convection is a critical process in the development and maintainance of the front. The meridional and zonal secondary circulations resulted from Mei-yu condensation heating both act to increase the wind speed in the LLJ. The condensation induced local circulation strengthens the moisture transport in the LLJ, providing a positive feedback to sustain the Mei-yu precipitation system. It is found that local precipitation recycling shifts heavy rain toward the warm side of the Mei-yu front. This shift of rainfall location is due to the pronounced increase of atmospheric moisture and decrease of surface temperature over the warm side of the front.

1. Introduction

The South China Sea Monsoon Experiment (SCSMEX) was carried out in the summer of 1998 to study the onset and evolution of the South China Sea (SCS) monsoon and its impacts on rainfall variability over Southeast Asia, southern China and adjacent regions (Lau et al. 1999). It was observed that during the break phase of the SCS monsoon in the first two weeks of June, 1998, torrential rain occurred over the Yangtze River, associated with the development of a Mei-yu front in central China (Ding and Li 1999). The heavy rain events which persisted throughout the summer of 1998 caused extensive flooding over central and northeastern China, exacted heavy toll on the livelihood of over large segments of the East Asian population, inflicting a total economic loss of over 12 billion US dollars (National Climatic Center Report, 1998).

The occurrences of major torrential rain over the Yantze River Valley (YRV) in the summer of 1998, as a major climate event, has been reported in a number of recent large-scale observational and general circulation modeling studies (Lau and Weng 2001, Lau and Wu 2001, Shen et al. 2001, Wang et al. 2000). In this paper, we use a coupled mesoscale atmosphere-land model to investigate the mechanisms of the torrential rain, the sources and sinks of moisture and the possible interaction between precipitation and land surface processes during the heavy rain period June 11-17, 1998. Since the development of the Mei-yu front is key to the heavy precipitation over YRV during summer of 1998, a brief review of Mei-yu moisture processes and an overview the June 1998 Mei-yu are provided in Section 2. Section 3 describes the numerical model and experimental setups. In Section 4, we will clarify the water vapor sources for the Mei-yu precipitation. Local precipitation recycling will be studied in Section 5. Section 6 gives the summary and discussions.

2. A Mei-yu primer

2.1 Mei-yu moisture processes

The Mei-yu is a quasi-stationary summer monsoon precipitation system over eastern Asia (Tao and Chen 1987). The unique large scale circulation pattern associated with the special topography of the Tibetan Plateau causes the Mei-yu front staying for a prolonged period (about two weeks to one month) along YRV. The interaction of several large scale systems, which are the moist southwestly monsoonal flow and the associated low-level jet (LLJ), dry northwestly from the north side of the Tibetan Plateau and the atmospheric subtropical high over the west pacific ocean, etc., form a large scale environment favoring Mei-yu system along YRV all the way east toward Japan. Three key issues relevant to this study, namely the moisture source, LLJ, and precipitation recycling, are briefly discussed below.

The first important issue is the tracking of moisture sources. Large scale circulation indicates that during northern summer most of the moisture in southeastern China is from the west and south direction (Simmonds et al. 1999). But it is not so obvious whether the moisture flux from the Bay of Bengal (BOB) or that from SCS is more important for the Mei-yu precipitation. For example, in the study of a Mei-yu flood case in the Sichuan basin (which is by the eastern side of the Tibetan Plateau) in 11-15 July 1981, Zhou and Hu (1984) and Chengdu Central Observatory (1982) suggested that the major moisture source for the flood was the SCS. But for the same case, Kuo et al. (1986) based on moisture flux calculations found that the moisture transport from BOB is considerably larger than that from the SCS.

Delineating moisture sources for Mei-yu precipitation is a subtle and delicate problem, largely depending on how to define the boundaries or interfaces on which the moisture fluxes are calculated. In earlier studies, these boundaries were often located close to the target precipitation region but far away from the moisture source regions. Chen et al. (1983a) calculated the moisture transport in the summer months of 1979 to 1981, and found that

the moisture in YRV is transported from the west and south boundaries of the basin, which were linked to the moisture sources from BOB and SCS, respectively. Their results showed that the moisture flux from the west boundary is larger than that from the south boundary in May and vise versa in June. However, not only is the length of the south boundary double the size of the west boundary, but also their positions at 26N and 105E are very close to YRV but far away from the moisture source regions. Therefore, it is hard to say whether the moisture flux at the south boundary is originally from SCS alone or from SCS and BOB combined. Shen (1983) studied atmospheric moisture transport and precipitation in YRV in July, and found that the moisture transport by the southwesterly monsoonal flow is stronger in wet years. However, he claimed that the moisture in the southwesterly monsoonal flow is mostly originated from SCS, enhanced by the land surface evaporation in southern China. Simmonds et al. (1999) compared the atmospheric water vapor fluxes and the summer precipitation of southeastern China in the domain of 25-35N and 110-120E, in wet and dry years. The averaged moisture inflow flux is larger on the south boundary than that on the west boundary. However, the wet-year flux is more than double of the dry-year flux in the west boundary (the difference is 177.9 $mm\ month^{-1}$), while in the south boundary the differences is only 92.3 $mm\ month^{-1}$. Hence, it is obvious that the precipitation in the southeastern China is more sensitive to the changes of moisture fluxes through the west boundary than to that through the south boundary. Notwithstanding their argument that most of the inflow increment may actually not from BOB but originally from SCS, their results indicate the importance of different moisture sources for the precipitation in the Mei-yu system. In fact, most of the moisture moves out of the southeastern China via east and north boundary without delivering any precipitation. Therefore, moisture sources that actually bring forth precipitation cannot be diagnosed by merely calculating water wapor fluxes across certain interfaces.

The second important issue is the relationship between Mei-yu and LLJ. The Mei-yu rainfall is statistically closely related to the LLJ southeastern to the Tibetan Plateau

(Chen and Yu 1988), and the correlation coefficient between the occurence of severe storm and LLJ is as high as 0.8 (Tao and Ding 1981). During Mei-yu season, the lower and middle troposphere over southeastern China is dominated by the southwesterly monsoonal flow. The LLJ is a maximum wind region located between 850 and 700hPa with a speed exceeding 15 ms^{-1} and a horizontal length scale of about 500km (Chen et al. 1998). It brings plenty of warm wet air from the subtropical oceans to southeastern China which fuels the precipitation in Mei-yu front. The generation and development of LLJ and the propagation of its wind speed maximum are, to a large extent, controled by the orographic effects of the plateau on the airflow along the west periphery of the subtropical high and on the amplification of low-level vortices. When the subtropical high stretches westward and at the same time a plateau-related vortex is developing, one often obverves the presence of a very strong LLJ reaching wind speeds of 20-25 $m\ sec^{-1}$. On the other hand, the latent heat release by precipitation can feedback with LLJ through local secondary circulations (Chen et al. 1998; Chen et al. 1994).

Another unknown problem in Mei-yu precipitation is the role of precipitation recycling, defined as the contribution of local evaporation to local precipitation (Brubaker et al. 1993; Eltahir and Bras 1996). The precipitation-induced surface evaporation and evapotranspiration increases atmospheric moisture, but the net effect of locally evaporated moisture on local precipitation is very much dependent on the "precipitation efficiency"–the fraction of moisture flowing through a region that is precipitated out, which is usually small in the southeastern China (Trenberth 1999). On the other hand, the local evaporation decreases the ground temperature, thus changes the thermodynamic structure of the atmosphere, and in turn affects the precipitation (Paegle et al. 1996; Beljaars et al. 1996).

2.2 Overview of June 1998 Mei-yu

In 1998 summer, the average precipitation in YRV was over 500 mm. Precipitation in some areas, such as Bo-yan Lake and Gan River in the middle reach of YRV, exceeded 1000 mm, and the precipitation anormaly was larger than 100%. The Mei-yu period began

in YRV on June 12. June 12-28 was one of the heavy rainy period. In Eurasia area, two blocking high patterns were found on the 500hPa height field; one over Ural Mountain, the other over Sea of Okhotsk, which was the typical circulation in high latitudes during Mei-yu period. In the northwesterly flow in the southwest flank of the Okhotsk block, cold airs frequently penetrated YRV. In the subtropics, a high pressure ridge was found over the Tibetan Plateau. The warm and moist air from the southwest or southeast side of the subtropical high confronted with the cold air from northwest, triggerred heavy precipitation in Mei-yu front (Zhang et al. 2001).

Figure 1 shows the observed TMI rain rate ($mm\ day^{-1}$) and 850hPa wind vector, from June 11 to 16, 1998. We observe that the Mei-yu front precipitation started on June 12. It became very strong and the center of the cyclonic belt moves to the line along (130E, 32N) and (110E, 28N) on June 13. The torrential rain occurred south of this line from June 12. The precipitation in YRV is relatively small on June 14, but rebuilt up on June 15 and 16. Note that the high values near the northwest corner of the domain do not really reflect high values of precipitation but are caused by the high-altitude topography of the Tibetan Plateau in the process of TMI data processing. In the 850hPa wind field, the strong southwesterly monsoonal flow persisted through the whole period of simulation from June 11 to 16 in southeastern China, with wind speed exceeding 15 m/sec over a vast area south to the Yangtze river. This strong southwesterly flow is referred to as the low-level jet. Strong southwesterly flow is also observed in BOB which is connected to the Indian monsoon system. However, the southwesterly wind speed in low level over southwestern China and the Indo-China Peninsula is small, due to the obstruction of the southeastern edge of the Yunnan-Guizhou Plateau. The 200hPa circulation (not shown) is dominated by the Southern Asian High pressure system, centered over the Tibetan Plateau. The Southern Asian High moves slightly eastward and the northwesterly wind in the northeast flank of it strengthened from June 11 to 13.

3. Model

The mathematical tool for this study is a coupled mesoscale atmosphere-land model (Lynn et al. 2001). The atmospheric component is the nonhydrostatic PSU-NCAR mesoscale model MM5 containing various boundary-layer, convection, and radiation parameterization schemes (Dudhia 1993; Grell et al. 1995). The land component is the NASA/GSFC PLACE model (Parameterization for Land-Atmosphere-Cloud Exchange, Wetzel and Boone 1995). Considered in PLACE are the subgrid surface heterogeneity and the feedbacks between soil, land surface, vegitation, and entraining shallow cumulus clouds. Therefore, soil moisture interacts with precipitation, evaporation, infiltration, runoff, and soil water drainage to bedrock. The coupled model, called MM5P, is used to investigate various aspects on the remote moisture sources, the interaction between precipitation and LLJ, and the local effect of precipitation-evaporation feedback in a Mei-yu precipitation event of June 11-17, 1998.

Instead of setting flux calculating interfaces close to YRV, we will set our model outer domain boundaries close to the moisture source regions of BOB and SCS. By directly reducing the moisture supply from each source region, we will be able to delineate their impacts on Mei-yu precipitation.

The double-nested model domains cover the southeastern Asia region on a Lambert conformal map shown in Fig. 2 as the shaded area. Topography is shown by contours. The outer domain D01 has 73x64 grids with ΔX=60km, centered at (120E, 27.5N). The southwest corner of the outer-domain is at (100E, 10N), nearby the southwest corner of the Indo-China Peninsula, so that the west boundary faces BOB and the south boundary is over middle SCS. In the atmospheric general circulation field, the southwest corner of the outer domain is roughly between the southwesterly LLJ and the flows south to the LLJ. We set the outer domain in such a way that the effect from BOB and SCS can be separated. The inner domain D02 has 136x109 grids with Δx=20km, which includes northern SCS, eastern China, and the adjacent ocean. The Mei-yu front is across the middle of the high-resolution inner domain in the east-west direction. Vertically, there are 23 atmospheric layers in MM5

and 5 soil layers for soil moisture in PLACE. Kain-Fritch convection scheme, Blackadar PBL scheme, Dudhia simple ice scheme and Goddard radiation scheme are chosen for parameterization. The model was run for a week from 0000UTC June 11 to 0000UTC June 18, 1998, with the time step of 3 min.

4. Largescale impact – remote moisture sources

4.1 Moisture sources

In this section, we will examine the remote moisture sources that physically deliver Mei-yu precipitation. For this purpose, five model runs are conducted: 1) control run CTRL, which is the coupled MM5 and PLACE with precipitation-evaporation interaction; 2) W80, in which the atmospheric water vapor flux in the west lateral buffer zone of the outer domain is reduced by 20 % (i.e., be 80 % of the control run); 3) S80, water vapor flux reduced by 20 % in the south buffer zone; 4) E80, water vapor flux reduced by 20 % in the east buffer zone; 5) W50, water vapor flux reduced by 50 % in the west buffer zone. The width of the lateral buffer zone is $5\Delta X$. The model setups for the later four runs are exactly the same as that of CTRL, except that the moisture flux along one side of the model outer domain is reduced by a certain percentage. Therefore, their differences from CTRL should reflect the impacts of remote moisture transport from various sources.

In the control run, the model captures the Mei-yu front rainfall pattern. The daily rain rate, 850hPa wind, 200hPa height and wind fields are shown in Fig. 3. We can see that a mature Mei-yu front formed on June 13. The 6-hour rain rates (not shown) indicate that Mei-yu front precipitation formed from 1800UTC, Jun 12, along the latitude of about 28N slightly tilted in the SWW-NEE direction, and that a number of precipitation centers, separated by 200-300km from each other, were propagating eastward along the Mei-yu front. At 200hPa, the eastern part of the Southern Asian High was over the model domain. Northeastern to the Southern Asian High was the strong northwesterly wind behand the eastern Asian trough. The trough moved to the eastern coast of China and

the northwesterly wind increased from June 11 to June 13, just as the observations. Very heavy rainfall was produced in the middle reach of YRV, where flood took place. Similar to the observations, the simulated Mei-yu rain belt evanesced on Jun 14, partly rebuilt up on 15, and fully recovered on 16. Compared to the TMI observation in Fig.1, we can see that the model successfully simulated the spatial pattern and time evolution of the Mei-yu system.

In the experiments of S80 and E80 in which the moisture fluxes from the south and east boundaries are reduced by 20%, respectively, the intensity of Mei-yu precipitation has not been reduced. However, the Mei-yu precipitation is remarkably reduced in the experiment of W80 (their comparisons to CTRL on June 13 will be shown in Fig. 5, shortly). Actually, if we further reduce the water vapor and its flux in the west boundary by 50 % (W50), the Mei-yu rain belt almost disappears. Figure 4 shows the daily rain rate and 850hPa wind from June 11 to 14 for the W50 case. Comparing to Fig. 3 of CTRL, we can see that the W50 precipitation in YRV is gradually reduced from the first day of simulation, and the Mei-yu precipitation almost totally disappeared on June 13. Hence, it is clear that the moisture that fuels the Mei-yu precipitation is mostly from BOB, transported by the southwesterly LLJ. These experiments also reveal that the Mei-yu precipitating moisture does not come from the equatorial region that transported across the south boundary of the outer domain at 10N. It also implies that the moisture evaporated over the northern SCS and the land area of southern China is not the major source for the precipitation in YRV in this case. Otherwise, the moisture evaporated over SCS and southern China would bring some precipitation so that the Mei-yu rainfall would not be absent in YRV in the W50 run. The evaporation over SCS will be calculated in Section 4.3.

4.2 Interaction between Mei-yu front and LLJ

We also see from Fig. 4 that the 850hPa southwesterly monsoonal flow in southeastern China in the W50 run is almost as strong as in CTRL, which implies that its formation is mostly contributed by large scale conditions rather than local latent heating. However,

as suggested by many studies (Chen et al. 1994; Chu and Chen 1995; Hsu and Sun 1994; Nagata and Ogura 1991; Chen and Chen 1995), the LLJ is also related to the local thermodynamic forcing. The relationship between condensation heating and LLJ are examined by analyzing the difference field between CTRL and other experiments. We plotted the difference fields of precipitation and 850hPa wind between CTRL and W50, W80, S80 and E80 in Fig. 5a,b,c and d, respectively, on June 13, when the Mei-yu front is mature. Figure 5a and b clearly show that, compared to CTRL, the Mei-yu precipitation is considerably reduced in W80 and almost totally removed in W50. Accordingly, a cyclonic local circulation is observed in the 850hPa wind difference field close and slightly west to the Mei-yu precipitation center. This local circulation is caused by the latent heat released in Mei-yu precipitation, and its strength is proportional to the precipitation amount by comparing Fig. 5a and b. South to the local vortex center there is a east wind component, therefore it will intensify the LLJ. In some grid points, the increase of the southwesterly wind speed can be as large as 5 m/sec. But the wind increase is small at most grid points far away from the Mei-yu rain belt in the LLJ region. We also see that the cross front component of the wind difference, which is basically ageostrophic, is larger than the along front component. This intensifies convergence into the Mei-yu rain belt. Therefore, the LLJ fuels the condensation, and in turn the condensation strengthens the LLJ as well as increases the convergence, forming a self-sustained system. In the difference field between CTRL and S80 (Fig. 5c), a weak cyclonic vortex is over SCS, which is induced by the moisture from the south boundary. The resulted wind difference in the LLJ region is opposite to the direction of the jet wind, therefore the moisture from the south boundary acts to slightly weaken the LLJ strength. The wind and precipitation differences between CTRL and E80 are very small (Fig.5d), indicating negligible moisture effect from the east boundary.

Next, let us look at the changes of Mei-yu front and LLJ in various vertical cross sections. In the meridional-vertical (yz) cross section of the equivalent potential temperature

(θ_e) and wind (v, w) fields averaged in the meridional belt of 114-121E (as shown in the four left panels of Fig. 6 from the second to the fifth day of simulation, i.e., June 12 to 15, 1998), the Mei-yu front is evident, as indicated by a maximum θ_e column, upward motion and lower-level convergence zone over about 29N. The zonal range of average from 114 to 121E is chosen because this is the major rainy area in YRV. The dry and cold air is in the north and the moist and warm air is in the south. Starting from June 13, they push together and form the Mei-yu front. In the corresponding figure for the W50 run (not shown), we can still identify the front-like convergence zone. However, the convergence is much weaker and more shallow, and the vertical motion is much smaller in W50 than those in CTRL. Therefore, the large scale background circulation dominates the dynamical formation of the Mei-yu front between northern cold and southern warm airs, but the moisture from BOB through the western boundary is crucial to fuel the moisture condensation and precipitation. The moisture contribution to the front and LLJ is manifested in the difference field between CTRL and W50 runs, as shown in the four right panels of Fig. 6, from June 12 to 15. The positive θ_e difference is in the frontal zone, with positive w difference. The latent heat release by condensation in the Mei-yu front induced meridional secondary circulations on both sides of the front, the indirect one with descending branch to the south and the direct one with descending branch to the north. In the begining two days (June 12 and 13), the θ_e difference is positive around 30N and it is concentrated between 25-30N on June 13, but later the descending air north to the front results in a negative θ_e difference, indicating increase of moisture gradient. Also, the increase of the northerly wind difference is rather large north to the front, particularly in low level, hindering the northward advancing of moist air and consequently the northward moving of the Mei-yu front. Therefore, the latent heating in the Mei-yu front introduces a positive feedback through the direct secondary circulation north to the front. In the indirect secondary circulation south to the front, a southerly differences are in the lower layers (execept for June 15). However, the difference is rather small (but according to Fig. 5a, the zonal average operation across 114-121E

may underestimate the real magnitude of the v difference). In a diagnostic study of the observed data of a Mei-yu case in TAMEX, Chen et al. (1994) also obtained similar results of a relatively strong direct and a weak indirect secondary circulations in the north and south sides of the Mei-yu front, respectively. By Coriolis effect, the southerly wind causes increase of westerly wind in the northerm hemisphere to conserve momentum. However, because the increase of v by the moisture process is weak, the increase of the westerly momentum by Coriolis effect should also be weak. Therefore, in this case, the momentum of the southwesterly LLJ cannot be adequately accounted for by the Coriolis effect of the meridional secondary circulations.

Then let us examine the zonal-vertical (xz) cross section of the θ_e and (u, w) fields and the differences between CTRL and W50 runs. Since the Mei-yu front is located around 28-29N in the middle and lower reaches of YRV, and the LLJ is south to the front during most of the simulation period, we plot two xz cross sections: one avearaged in the zonal belt of 25-28N and the other avearaged in 28-29N (Fig. 7). The left four panels are θ_e and wind of CTRL run, and the right four panels are the differences between CTRL and W50 runs. From Fig. 7, we can see the whole layer from bottom to top is dominated by westerly wind, with southerly component under about 400hPa level and northerly component in the upper layers as seen from the yz cross section Fig. 6. The westerly flows downslope following the topography in the eastern flank of the Tibetan Plateau, then ascends at a certain distance to the east associated with condensation heating in the lower layers and the upward motion ahead of the Eastern Asian Trough in the upper layers. In the difference fields between CTRL and W50, we can clearly see the effect on the θ_e and wind velocity by moisture imported from the west boundary, by the southwesterly LLJ. Accompanied the transport of the warm and moist air from the west is the upward motion by the condensation heating. Easterly returning flow can be seen in the difference wind field in the upper layers, therefore forming a zonal secondary circulation. This zonal secondary circulation slightly increases the downslope westerly wind from the Plateau. The LLJ is also strengthened in the middle

and lower reaches of YRV around 115-125E in the 25-28N zonal belt, by as large as about 5 m/sec on June 14, for example. The westerly wind increase is remarkable in the front edge east of the precipitation center, in the lower and middle troposphere, by a difference exceeding 5 m/sec. However, in the west part of the zonal belt of 28-29N, we see the easterly wind difference on 850 and 900 hPa levels. To the south, the corresponding wind difference in the west part of 25-28N belt is small, reflecting a horizontal cyclonic wind shear in the difference field.

Let us examine the vertical variation of the horizontal wind. In the left panels of Fig. 6, we can see that the southerly wind (v) is strong in lower troposphere (900 and 850hPa) but very weak in the middle troposphere (700-400hPa). In contrast, in the left panels of Fig. 7, the westerly wind (u) is strong not only in the lower troposphere but also in the middle troposphere. Hence, the northward atmospheric transport of moisture is confined in the lower troposphere, but the easterward transport of moisture is in the middle as well as lower troposphere. This is consistent with the diagnosed moisture flux directions of Ma and Bosart (1987) for a June 1983 Mei-yu case, in which the moisture flux is northward in the lower troposphere but northeastward in the middle troposphere. In fact, middle tropospheric transport is important for the moisture from BOB to pass over the southeastern edge of the Yunnan-Guizhou Plateau to reach YRV.

To study the impact of moist processes on the development and maintenance of the maximum positive vorticity belt along the Mei-yu front, we plotted the 850hPa vertical relative vorticity field for CTRL and its difference with W50 at 00UTC on Jun 12, 14, 16 and 18 (Fig. 8). By comparing the left panels with the corresponding right panels, we find that significant part of the positive vorticities (cyclonic wind shear) along the Mei-yu front are caused by the latent heat release by moist condensation in the Mei-yu front. The positive vorticity belt is narrow and concentrated along about 30N. The positive vorticity is much weaker in the W50 run (not shown). Williams et al. (1981) also found in his numerical experiment that frontal zones and the associated cyclonic shears are strengthened above

the planetary boundary layer by condensation heating. Our results is also consistent with Chen and Chang (1987) in that the cyclonic vorticity is due to Ekman pumping in the continental portion of the Mei-yu front. The location of the positive vorticity is shifted north in the W50 run in later days. As discussed early in the yz cross section Fig. 6, the direct meridional secondary circulation produces strong northerly wind in the lower layers, helps to maintain the quasi-stationary position of the Mei-yu front. Therefore, the condensation heating mechanism in the Mei-yu front is crucial to sustain both the strength and the quasi-stationary position of the front. In this sense, the continental part of the Mei-yu front is much like the quasi-barotropic convection in the tropics (Chen and Chang 1980). However, different from in the tropics, the Coriolis effect cannot be neglected here in YRV. Thus, latent heating results in a cyclonic wind shear of secondary circulation, unlike that in the tropics.

4.3 Water budget analysis

To quantify the moisture processes, we calculated the model's hydrology budget by horizontally and vertically integrating the continuity equation of atmospheric moisture around a rectangular domain (Bosilovich and Sun 1999), which yields:

$$W = FW - FE + FS - FN + E - P - R, \tag{1}$$

where W is the total change of atmospheric water vapor which is generally a small term; FW, FE, FS, and FN are the vertically integrated moisture fluxes along the west, east, south, and north boundaries of the budget calculation domain, respectively; $Q = FW - FE + FS - FN$ is the total moisture convergence in this area; E is the total surface evaporation; P is the total precipitation; and R is the residual term. Water budgets are calculated over four rectangular domains A, B, C, and D, representing western China, YRV and southern China, SCS, and the Indo-China Peninsula, respectively (Fig. 9). To test the model sensitivity to moisture source, it is desirable to keep the atmospheric momemtum field be as close as possible to the control run. Therefore, we compared the budget components

of W80, S80 and E80 in which the magnitude of moisture transport at a lateral boundary is only reduced by 20% so the momemtum field is not twisted too much. The values in Fig. 9 are those averaged from 36hr through 144hr in the time integration of the model, considering the time needed for the initial and continuous moisture changes at the outer boundary of the domain to affect precipitation in the inner region of the domain over YRV. Also note that the values in Fig. 9 is the total sum over each budget calculation domain, in the unit of 10^6 Kg/sec of water, and here we are only interested in the relative changes of their values. Each budget component is shown in the middle, while the difference values for S80-CTRL, W80-CTRL, and E80-CTRL are below and on the left and right hand side of the CTRL value. The value above the CTRL one is for the non-feedback case for precipitation recycling which will be discussed in section 5. The values of E, W, and R do not vary much among different experiments, therefore, only the values in CTRL case are given in Fig. 9. The total atmospheric water vapor change W is small. The change of cloud water storage is included as part of the residule term R. For domain B, the CTRL total precipitation P is 144, the surface evaporation E is 45, the total moisture fluxes FS, FW, FN, and FE are 280, 450, -65, and 689, respectively, thus the moisture convergence Q is 105. The B/C interface roughly devides continental China and SCS. So the fluxes accross this boundary, 280, is the moisture source from SCS. This flux is contributed over domain C by the surface evaporation (83), the transport from tropical oceanic source (191), the subtropical western pacific source (133) and the Indo-China Peninsula source (46). Note that the moisture transport from Indo-China Peninsula to SCS is rather small. Most moisture over domain B comes from its west boundary (from A to B), and it is further derived mostly from domain D, by the southwesterly LLJ. For the W80 case, FW of domain D and A are reduced by 54 and 35, respectively, and FW of domain B is reduced by 51, the precipitation over B is reduced quite substantially by 38 (about 1/4 of P of CTRL). Therefore, Mei-yu precipitation is very sensitive to BOB moisture source. For the S80 case, FS of domain C and D are reduced by 73 and 49, respectively, and FS of

B is reduced by 25, but the precipitation over B is only reduced by 4. Note that FW of B increases by 16 in S80 case, indicating the strengthening of LLJ in S80 as can be seen from Fig. 5c. Thus, although the moisture tranport from the tropics is quite strong, its impact on Mei-yu precipitation is small. The moisture that fuel the Mei-yu precipitation is mostly from the west boundary of domain D, facing BOB. The budget calculation also confirms that the moisture from the Pacific ocean (E80 case) has little effect on Mei-yu precipitation.

5. Mesoscale impact – local precipitation recycling

5.1 Impact on rainfall distribution

We conducted an experiment by turning off the precipitation-surface evaporation interaction (or non-feedback, denoted by NF) in the land-surface model PLACE. In NF run, the precipitation has no impact on the land-surface processes, or the precipitation is totally running off immediately. The NF run is compared to the control run (CTRL) in which the contribution of local precipitation to the surface evaporation is retained. Since every other things in the model runs are exactly the same, the difference between CTRL and NF represents the effect of local precipitation recycling from the land surface. Precipitation differences and the energy and water vapor budgets are analyzed in the vicinity of the Mei-yu front region with 20km-grid resolution of the model inner domain during the mature stage of Mei-yu front. The 6-hour rain rate (contour) and the time-averaged 850 hPa wind (vector) fields are shown for the 4 quarters of June 13, in Fig. 10 for CTRL, Fig. 11 for NF, and Fig. 12 for their difference (CTRL-NF). The top two panels are for 00-06UTC and 06-12UTC, corresponding to 8am-2pm and 2pm-8pm on June 13 of the Local Standard Time (LST, which is Beijing time), respectively, hence approximately being local daytime. The bottom two panels are for 12-18UTC and 18-24UTC, corresponding to 8pm June 13 to 2am June 14 and 2am-8am June 14 of Beijing time, respectively, being local nighttime. A cyclonic wind shear line is along about 29N, between weak northwesterly in the north

and strong southwesterly in the south. The heavy precipitation belt is located south to the wind shear line. The north-south width of the Mei-yu rainbelt is about 2 degrees of latitude, or approximately 200km. Several maximum precipitation centers are found in the Mei-yu precipitation belt. The maximum value can reach 50 $mm\ 6hr^{-1}$, as shown in Fig. 10c and d. Note that the strong precipitation in the nighttime of June 13 is not typical for other days in the simulation, therefore, it is not caused by the nocturnal strengthening of upstream LLJ proposed by Paegle et al. (1997) for the 1993 US midwest flood. The simulated precipitation in the Mei-yu front belt is contributed mostly by stable precipitation part and minorly by convective precipitation part. For CTRL case, in daytime (particularly in the afternoon), minor precipitation centers (about 100km scale) are seen south to the Mei-yu front. For example, we see a train of three local minor precipitation centers along the southeastern coast of China, in the strong southwesterly flow. Numerical results show that these minor precipitation centers are contributed by convective precipitation part. North to the Mei-yu front, there is also a vast area of light precipitation, contributed by the stable precipitation part. In contrast, these minor precipitations on both sides of the Mei-yu front are absent in the NF case, as shown in Fig. 11. This is also manifested in the difference field in Fig. 12 (between Figs. 10 and 11). Therefore, these minor precipitations are caused by the addition of surface evaporation contributed by local precipitation, i.e., precipitation recycling. By checking the CTRL precipitation distribution on June 11 and 12 (not shown), we notice several convective precipitation centers did exist in the same locations as those minor precipitation centers on June 13 along the southeastern coast of China, proving the significance of the precipitation recycling of the previous days to these local rainy vortexes. Eltahir and Pal (1996) also noticed the relationship between surface conditions and the subsequent rainfall. The temperature is highest and evaporation is strongest in the afternoon, therefore those minor precipitation centers also show diurnal variation, with maximum in the afternoon. We compared CTRL and NF precipitation for

all seven days in the simulations, and the minor precipitation centers are all absent in the NF run, thus above result is robust.

However, the major precipitation differences between CTRL and NF runs are in the Mei-yu front itself, as can be seen in Fig. 12. In Fig. 12a, b, and c, the role of precipitation recycling is to increase precipitation in the southern half of the Mei-yu rain belt and decrease the precipitation in the northern half of the rain belt. In some local region, the differences can be as large as 30 $mm\ 6hr^{-1}$. Therefore, the maximum rain belt shifted to the south in the first three quarters of June 13. In Fig. 12d, the rainbelt slightly shifted to the northwest. The maximun rainfall location shift is also indicated in daily rainfalls.

Figure 13 shows the meridional distribution of daily precipitations zonally averaged between 114E and 121E over YRV, from June 11 to 17. The solid line is the daily rain rate for CTRL, dashed line for NF. The observed TMI precipitation data is also plotted for reference, by the dash-dot-circle line. First, we see differences from model simulated precipitations to the observed ones. In the first two days, the model delayed to produce large amount of rainfall over the vast area north to 29N. The simulated rainfall on June 12 in some extent reflects the actual rainfall of June 11. However, the Mei-yu front formed on June 13, and its intensity and location are close to the observation. With the increase of simulation time, the differences between CTRL and NF runs increases. However, the precipitation in CTRL run is closer to the observation than that of NF run. Overall, the model produced the Mei-yu precipitation and simulated its temporal variation reasonably well. It must be emphasized, however, that the point of this study is not to verify the accuracy of a forecast but to simulate changes produced by precipitation-evaporation interaction. Therefore, we just compare the differences between CTRL and NF in the following analysis.

5.2 Mechanism analysis

To understand why precipitation recycling relocates heavy precipitation, we compared surface heat fluxes between CTRL and NF. Figure 14 gives the CTRL surface latent heat flux (LHFX, contoured) and its difference to that of NF [LHFX(CTRL-NF), shaded]. The

diurnal variation is obvious, with maximum LHFX and LHFX(CTRL-NF) in the daytime and their minima in the night. Since the magnitude of LHFX is much larger in the day than in the night, the daily averaged values are dominated by their daytime values. It is also clear that LHFX as well as its diurnal variation are very small along the Mei-yu precipitation belt. This is reasonable because the atmosphere is almost saturated over the Mei-yu rainbelt, hence the evaporation should be small. The meridional distribution of latent and sensible heat fluxes, zonally averaged in 114E to 121E, are shown in Fig. 15. First, we can see that the LHFX is much larger than SHFX in CTRL. In NF, the soil is dried up by removing precipitation in the land-surfaces processes. Therefore, the latent heat flux in CTRL (thick solid line) is larger than that in NF (dashed line), but vise versa for the sensible heat flux (SHFX). However, the opposite-signed differences are not exactly compensated in the total surface heat flux. Comparing to the meridional distribution of precipitation in Fig. 13, it is indeed that the LHFX difference is the smallest at the maximum precipitation center where the relative humidity is the highest and the atmosphere is almost saturated thus hindering evaporation. But the LHFX difference is larger on the two sides of the rainbelt, particularly on the south side where the surface temperature is higher and the near-surface wind is stronger thus promoting evaporation. The SHFX difference between CTRL and NF is also small over the Mei-yu precipitation belt, but the magnitude of the difference is larger north to the Mei-yu front where stable precipitation (although it is light in CTRL) and the associated clouds are removed by turning off precipitation recycling in the NF run. Figure 16 shows the meridional distribution of the surface temperature averaged between 114E to 121E (with calibration on the right ordinate in K). It is obvious that the surface temperature in CTRL is smaller than that in NF, due to more precipitation-induced evaporation in the former. Since the evaporation is stronger when temperature is higher, the moisture and temperature changes are larger over warmer surfaces. Therefore, we also plotted the precipitation difference between CTRL and NF in Fig. 16 (with calibration on the left ordinate in $mm\ day^{-1}$). We can see in general that negative precipitation differences

are over the region of minimum surface temperature but positive precipitation differences are over warm region, which means heavy precipitation are shifted to the warmer sides in the Mei-yu front. On June 13, for example, heavy precipitation centers shifted to the south side of the Mei-yu front where surface temperature is higher, so that more moisture is evaporated and surface temperature is more decreased in CTRL, and the atmosphere becomes easier to saturate, hence produce more precipitation.

Finally, let us examine the impact of precipitation recycling on the total precipitation amount. The differences of water budgets between NF and CTRL are given in Fig. 9, where the values are averaged from 36hr to 144hr of simulation and in the unit of 10^6 Kg/sec. In domain B, the YRV and southern China region where Mai-yu torrential rain occurs, the evaporation is reduced by 12 (or 27%) by turning off the precipitation recycling. The precipitation in this domain is reduced by 8 in NF run. In domain C or SCS, the ocean surface evaporation is hardly affected by the land-surface scheme. In contrast, in the continental region domain A (western China), although the evaporation is only moderately reduced by 7 (or 13%) in NF run since torrential rain is not in this area, the local precipitation decrease is 16 (or 28%), being most sensitive to the recycling. In the Indo-China Peninsula and its adjacent ocean region (domain D), the sensitivity of precipitation to its recycling is medium.

6. Summary and discussions

By placing our outer model domain boundaries close to the moisture sources, with south boundary over SCS, and west boundary facing BOB, respectively, we can delineate the impacts of moisture transfer from them. The numerical results show that the moisture that delivers the Mei-yu precipitation in YRV is mostly derived from BOB, transported by the southwesterly monsoonal flow passing over the southeastern edge of the Yunnan-Guizhou Plateau. In this case study, the Mei-yu precipitation is not produced by the moisture from SCS. Our modeling results agree with the synoptic analysis of Ma and Bosart (1987) for

the Mai-yu case of 23-25 June 1983 as well as the climate diagnostic study of Simmonds et al. (1999). These studies suggest that the precipitation efficiency by the moisture from BOB is higher than that from SCS for Mei-yu in YRV.

Considering summer wind directions and the physical distances from moisture source region to precipitation region, it seems reasonable to speculate that the precipitation in southwest China and YRV is more subject to the impact of the moisture from BOB, but the precipitation in southern China (particularly Guandong and Guanxi provinces) is prone to the effect from SCS. That is, for southern China, the precipitation efficiency of the moisture from SCS could be higher than that from BOB. It would be worthwhile to apply similar modeling approach to that used here to the early summer Mei-yu precipitation cases over southern China.

The absence of precipitation in W50 case provides us an opportunity to study the interaction among condensation heating by Mei-yu precipitation, LLJ, and the cyclonic shear or high relative vorticity along the Mei-yu front, by comparing to CTRL simulation. In W50 run, although the heavy precipitation belt is absent in YRV, the 850hPa southwesterly monsoonal flow over the vast area of the Southeastern China is still present and its strength is similar to that in CTRL run. This reveals the significance of the background large scale circulation for Mei-yu development, such as the interactions among the northwestward stretching of the subtropical high, the topographic blocking of the Tibetan Plateau, and the northwesterly flow from the north side of the Tibetan plateau, etc. However, in the vicinity of the Mei-yu front in YRV, the condensation heating by Mei-yu precipitation produces local cyclonic mesoscale circulations in the low level to enhance the convergence and therefore strengthen the precipitation itself. The Mei-yu latent heating also causes a zonal-vertical secondary circulation between the eastern edge of the Tibetan Plateau and the heavy precipitation center in YRV, adding eastward wind component in the low level to increase the southwesterly LLJ. The low-level northward component in the indirect meridional-vertical secondary circulation south to the Mei-yu front also acts to increase westerly

momentum in the LLJ by the Coriolis effect. Therefore, the latent-heating-induced local mesoscale circulation contributes to the formation of LLJ in the southwesterly monsoonal flow and the increased LLJ in turn enhances the Mei-yu precipitation, forming a positive feedback. The latent-heating-induced direct meridional-vertical secondary circulation north to the Mei-yu front is stronger than the above indirect one, creating strong northerly wind component in the low level behind the Mei-yu front. In Mei-yu period, precipitation front usually keeps quasi-stationary position in YRV for a prolonged time. The strong low-level northerly wind in the direct secondary circulation may be one of the causes in hindering the northward advancing of the Mei-yu front. We indeed found that the positive (cyclonic) relative vorticity belt along the Mei-yu front is not only stronger in intensity but also more stationary in position in the CTRL run than that in the W50 run.

Our numerical results indicate that one impact of precipitation recycling is to shift the location of the heavy precipitation centers. In this case, there is no major precipitation along the path of the southwesterly LLJ before it reaches YRV, hence saving plenty moisture from BOB for Mei-yu precipitation. However, precipitation recycling modifies local thermodynamic structures by increasing atmospheric moisture content and in the same time decreasing ground temperature through surface evaporation of the precipitation, and this effect is more pronounced over warmer places. Therefore, precipitation recycling acts to shift the precipitation centers toward the warmer side of the Mei-yu front, usually to souther locations.

It is noted that in this one-week simulation case, precipitation recycling acts to increase precipitation in local and adjacent regions. For long-term climate variation, the effect of precipitation recycling should be even more important. Although the precipitation recycling ratio (defined as the relative contribution of the recycled precipitation to total precipitation) is smaller in Euroasia than that in North and South America and Africa, it can still reach about 0.1 in winter months and 0.2 in summer months (Brubaker et al. 1993). Besides the natural process of precipitation recycling, the human activity of irrigation also enhance

surface evaporation. Actually, China has the largest irrigated area in the world, and much of this is in the form of flooded puddy fields, particularly in summer months in southern China (Simmonds et al. 1999). Therefore, it deserves further investigations for the problem of precipitation recycling in the context of regional land-atmosphere-climate system.

Acknowledgment

We wish to thank Drs. Peter Wetzel, Xiaofan Li, Yansen Wang and Ms. Yiqin Jia for their help and discussion. The study is supported by the NASA RELACS project.

References

Beljaars, A.C.M., P. Viterbo, M.J. Miller, and A.K. Betts, 1996: The anomalous rainfall over the United States during July 1993: Sensitivity to land surface parameterization and soil moisture anomalies. *Mon. Wea. Rev.,* **124**, 362–383.

Bosilovich, M.G., and W.-Y. Sun, 1999: Numerical simulation of the 1993 midwestern flood: land-atmosphere interactions. *J. Clim.*, **12**, 1490–1505.

Brubaker, K.L., D. Entekhabi, and P.S. Eagleson, 1993: Estimation of continental precipitation recycling. *J. Clim.,* **6**, 1077–1089.

Chengdu Central Observatory, 1982: A study of Sichuan extraordinary heavy rainfall in July 1981. *Collected papers of Sichuan basin heavy rainfall in 1981*, Sichuan Meteorological Bureau, Chengdu, China, 12–37 (in Chinese).

Chen, C., W.-K. Tao, P.-L. Lin, G.S. Lai, S.-F. Tseng, and T.-C. C. Wang, 1998: The influence of the low-level jet during the development of mesoscale convective systems on a Mei-yu front. *Mon. Wea. Rev.,* **126**, 349–371.

Chen, G.T.J., and C.-P. Chang, 1980: The structure and vorticity budget of an early Summer monsoon trough (Mei-Yu) over southeastern China and Japan. *Mon. Wea. Rev.,* **108**, 942–953.

Chen, G.T.-J. and C.-C. Yu, 1988: Study of low-level jet and extreamly heavy rainfall over northern Taiwan in the Mei-yu season. *Mon. Wea. Rev.,* **116**, 884–891.

Chen, S.X., S.F. Gao, and S. Yang, 1983a: The source of water vapor in the southern part of China in May and June and its abnormability. *Proc. of the symposium on the summer monsoon in southeastern Asia,* People's Press of Yunnan Province, 97–110 (in Chinese).

Chen, S.X., S.F. Gao, S. Yang, and Y.Q., Guo, 1983b: The transport and balance of water vapor in the area south of the Yangtze River in May and June. *Proc. of the symposium on the summer monsoon in southeastern Asia,* People's Press of Yunnan Province, 111–122 (in Chinese).

Chen, X. A., and Y.-L. Chen, 1995: Development of low-level jets during TAMEX. *Mon. Wea. Rev.,* **123**, 1695–1719.

Chen, Y.-L., X.A. Chen, and Y.-X. Zhang, 1994: A diagnostic study of the low-level jet during TAMEX IOP 5. *Mon. Wea. Rev.,* **122**, 2257-2284.

Chu, H.-R., and G. T.J. Chen, 1995: Mei-yu frontogenesis. *J. Atmos. Sci.,* **52**, 2109–2120.

Ding, Y., and C. Y. Li, 1999: *Onset and activities of the South China Sea Monsoon and its interactin with the ocean* (in Chinese). Chinese Academic Press, 422 pp.

Dudhia, J., 1993: A nonhydrostatic version of the Penn State-NCAR mesoscale model: validation tests and simulation of an Atlantic cyclone and cold front. *Mon. Wea. Rev.,* **121**, 1493–1513.

Grell, G.A., J. Dudhia, and D.R. Stauffer, 1995: A discription of the fifth-generation Penn State/NCAR mesoscale model (MM5), *NCAR/TN-398+STR,* pp117.

Hsu, W.-R., and W.-Y. Sun, 1994: A numerical study of a low-level jet and its accompanying secondary circulation in a Mei-yu system. *Mon. Wea. Rev.,* **122**, 324–340.

Eltahir, E.A.B, and R.L.Bras, 1996: Precipitation recycling. *Rev. Geophys.,* **34**, 367–378.

Eltahir, E.A.B, and J.S. Pal, 1996: Relationship between surface conditions and subsequent rainfall in convective storms. *J. Geophys. Res.,* **101**, 26237–26245.

Kuo, Y.-H., L. Cheng, and R. Anthes, 1986: Mesoscale analyses of the Sichuan flood catastrophe, 11-15 July 1981. *Mon. Wea. Rev.*, **114**, 1984–2003.

Lau, K. M., Y. Ding, J. T. Wang, R. Johnson, T. Keenan, R. Cifelli, J. Gerlach, O. Thiel, T. Rickenbach, S. C. Tsay, and P. Lin, 1999: A report of the field operations and early results of the South China Sea Monsoon Experiment (SCSMEX). *Bull. Am. Meteor. Soc.*, **81**, 1261–1270.

Lau, K. M., and H. Weng, 2001: Coherent modes of global SST and summer rainfall over China: an assessment of the regional impacts of the 1997-98 El Nino. *J. Climate*, **14**, 1294–1308.

Lau, K. M., and H.T. Wu, 2001: Intrinsic modes of coupled rainfall/SST variability for the Asian summer monsoon: a re-assessment of monsoon-ENSO relationship. *J. Climate*, **14**, 2880–2895.

Lynn, B.H., D.R. Stauffer, P.J. Wetzel, W.-K. Tao, P. Alpert, N. Perlin, R.D. Baker, R. Munoz, A. Boone, and Y. Jia, 2001: Improved simulation of Florida summer convection using the PLACE land model and a 1.5-order turbulence parameterization coupled to the Penn State-NCAR mesoscale model. *Mon. Wea. Rev.*, **129**, 1441–1461.

Ma, K.-Y., and L.F. Bosart, 1987: A synoptic overview of a heavy rain event in Southern China. *Wea. Forcast.*, **2**, 89–112.

Nagata, M., and Y. Ogura, 1991: A modeling case study of interaction between heavy precipitation and a low-level jet over Japan in the Baiu Season. *Mon. Wea. Rev.*, **119**, 309–1336.

National Climate Center Report: 1998: *Severe flood and anomalous climate in China during 1998* (in Chinesee). China Meteorological Administration. Meteorology Press, 139pp.

Paegle J., K.C. Mo, and J. N. Paegle, 1996: Dependence of simulated precipitation on surface evaporation during the 1993 United States summer floods. *Mon. Wea. Rev.*, **124**, 345–361.

Shen, J.Z., 1983: Atmospheric water vapor budget in Summer monsoon over China. *Proc. of the Symposium on the Summer Monsoon in southeastern Asia,* People's Press of Yunnan Province, 147–157 (in Chinese).

Shen, X., M. Kimot., A. Sumi, A. Numagauti, and J. Matsumoto, 2001: Simulation of the 1998 East Asian summer monsoon by the CCSR/NIEW AGCM. *J. Meteor. Soc. Japan*, **79**, 741–757.

Simmonds I., D. Bi, and P. Hope, 1999: Atmospheric water vapor flux and its association with rainfall over China in Summer. *J. Clim.*, **12**, 1353–1367.

Tao, S.-Y., and L.-X. Chen, 1987: A review of recent research on the east Asian Summer monsoon in China. *Monsoon Meteorology,* C.P. Chang and T.N. Krishnamurti, Eds., Oxford University Press, 60-92.

Tao, S.-Y., and Y.-H. Ding, 1981: Observational evidence of the influence of the Qinghai-Xizang (Tibet) plateau on the occurrence of heavy rain and severe convective storms in China. *B. Americ. Meteor. Soc.*, **62**, 23–30.

Trenberth, K.E., 1999: Atmospheric moisture recycling: role of advection and local evaporation. *J. Clim.*, **12**, 1368–1381.

Wang, H.-J., T. Matsuno, and Y. Kurihara, 2000: Ensemble hindcast experiments for the flood period over China in 1998 by use of the CCSR/NIES AGCM. *J. Meteor. Soc. Japan*, **78**, 357–365.

Wetzel, P.J., and A. Boone, 1995: A Parameterization for Land-Atmosphere-Cloud Exchange (PLACE): Documentation and testing of a detailed process model of the partly cloudy boundary layer over heterogeneous land. *J. Clim.*, **8**, 1810–1837.

Williams, R.T., L.C.Chou, and C.J. Cornelius, 1981: Effects of condensation and surface motion on the structure of steady-state fronts. *J. Atmos. Sci.*, **38**, 2365–2376.

Zhang, S., S. Tao, Q. Zhang, and X. Zhang, 2001: Severe flooding in China during the summer of 1998. (in Chinese).

Zhou, X.-P., and X.-F., Hu, 1984: A brief analysis and numerical simulation of the Sichuan extraordinarily heavy rainfall event. *Proc. First Sino-American Workshop on Mountain Meteorology,* The Chinese Academy of Science and the U.S.National Academy of Science, Beijing, Amer.Meteor.Soc., 555-565.

Figure Captions

Figure 1: Observed TMI rain rate ($mm\ day^{-1}$, data only available in the shaded area) and 850hPa wind, June 11-16, 1998.

Figure 2: Model outer domain D01, inner domain D02, hydrology budget calculation domains A, B, C, and D, and topography (m).

Figure 3: Height (m) and wind on 200hPa pressure surface (left panels), and daily rain rate ($mm\ day^{-1}$) and 850hPa wind (right panels), for control run CTRL, June 11-16, 1998.

Figure 4: Daily rain rate ($mm\ day^{-1}$) and 850hPa wind for W50, June 11-14, 1998.

Figure 5: Differences of daily rain rate ($mm\ day^{-1}$) and 850hPa wind between control run and those with reduced moisture flux on one side of the outer boundary: (a) CTRL-W50, (b) CTRL-W80, (c) CTRL-S80, and (d) CTRL-E80, June 13, 1998.

Figure 6: Meridional-vertical (yz) cross section, averaged from 114E to 121E, of the CTRL equivalent potential temperature θ_e and (v, w) wind (left panels), and their differences with W50 (right panels), June 12-15,1998.

Figure 7: Zonal-vertical (xz) cross section, averaged from 25N to 28N (lower 4 panels) and from 28N to 29N (upper 4 panels), of the CTRL equivalent potential temperature θ_e and (u, w) wind (left panels), and their differences with W50 (right panels), June 12 and 14, 1998.

Figure 8: Vertical relative vorticity in CTRL (left panels), and its difference with that in W50 (CTRL-W50, right panels), at 00UTC June 12, 14, 16 and 18, 1998.

Figure 9: Water budgets in four domains A, B, C, and D (defined in Fig. 2), representing western China, Yangtze River Valey and southern China, South China Sea, and Indo-China Peninsula, respectively. Budget components P, E, Q, W and R are defined in Eq.(1). The unit is 10^6 Kg/sec.

Figure 10: CTRL 6-hour rain rate and 850hPa wind on June 13, 1998. The times in the brackets are the local standard times (LST) corresponding to the UTC ones.

Figure 11: Same as Fig.10, except for NF, the run without precipitation-surface evaporation interaction.

Figure 12: Difference between Fig.11 and 12 (CTRL-W50).

Figure 13: Meridional distribution of daily rain rate ($mm\ day^{-1}$), averaged from 114E to 121E: TMI observation (dot-dash-circle), CTRL (solid), and NF (dash).

Figure 14: Surface latent heat flux ($W\ m^{-2}$) for CTRL (contoured), and the difference between CTRL and W50 (shaded), for the four quarters of June 13, 1998.

Figure 15: Meridional distribution of the surface sensible (SHFX) and latent (LHFX) heat fluxes ($W\ m^{-2}$), averaged from 114E to 121E: CTRL LHFX (thick solid), NF LHFX (dash), CTRL SHFX (thin solid), and NF SHFX (dot).

Figure 16: Meridional distribution of ground temperature (K) for CTRL (solid) and NF (dash), and the difference of daily rain rate between CTRL and NF ($mm\ day^{-1}$, circle), averaged from 114E to 121E.

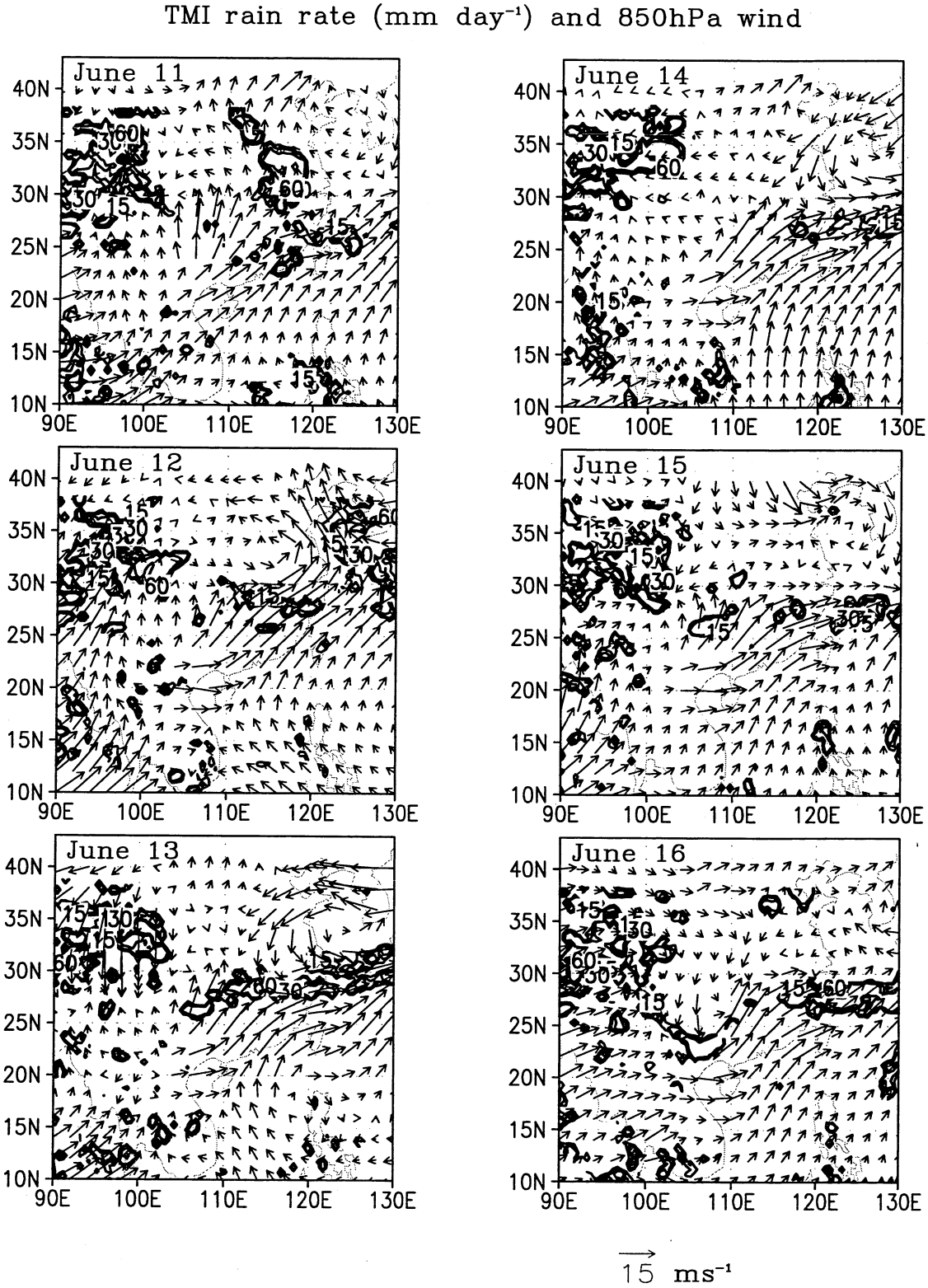

Fig.1 Observed TMI rain rate (mm day^{-1}) and 850hPa wind, June 11–16, 1998.

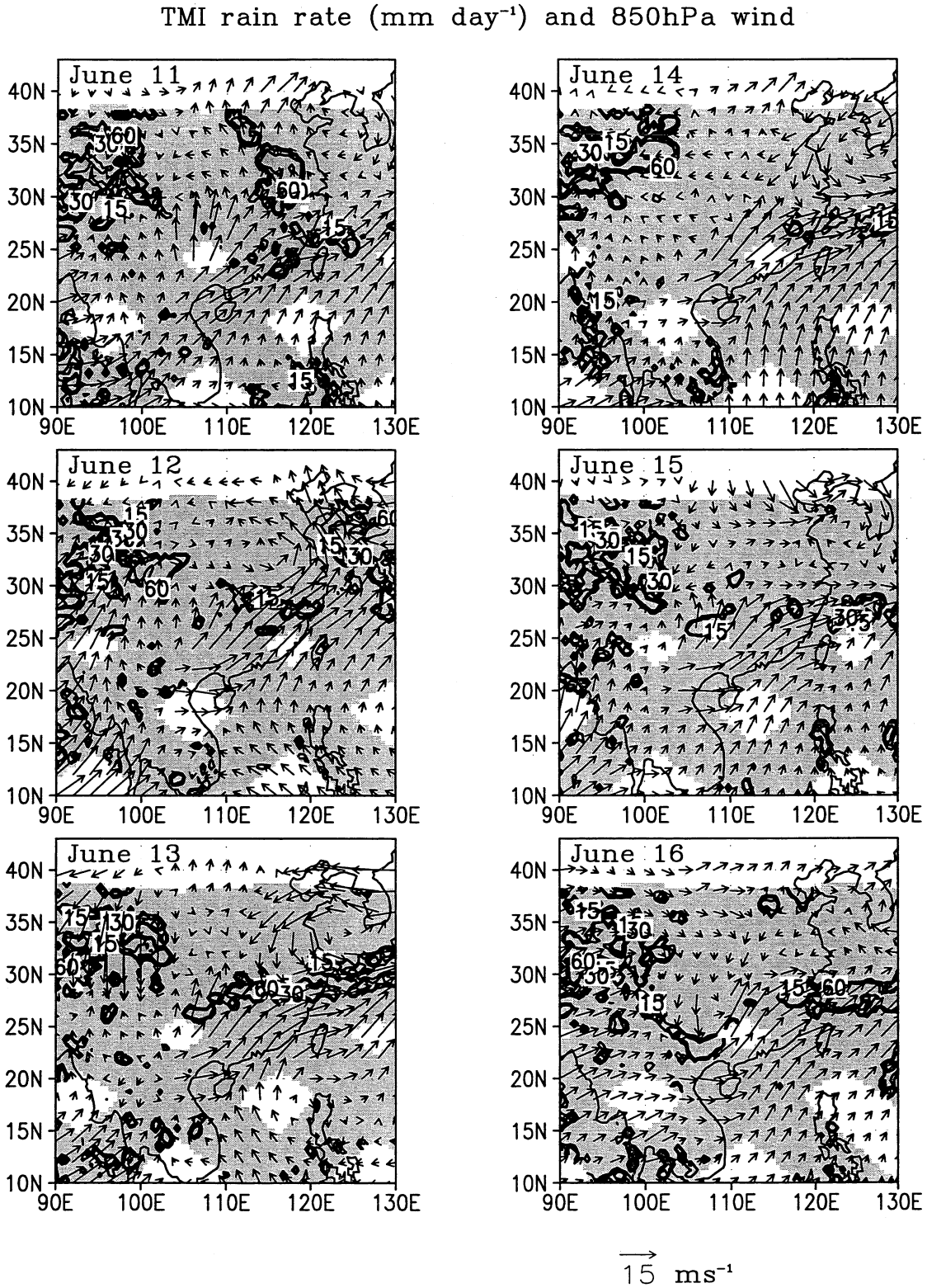

Fig.1 Observed TMI rain rate (mm day^{-1}, data only available in the shaded area) and 850hPa wind, June 11–16, 1998.

MM5P domains D01, D02; budget domains A, B, C, D; topography (m)

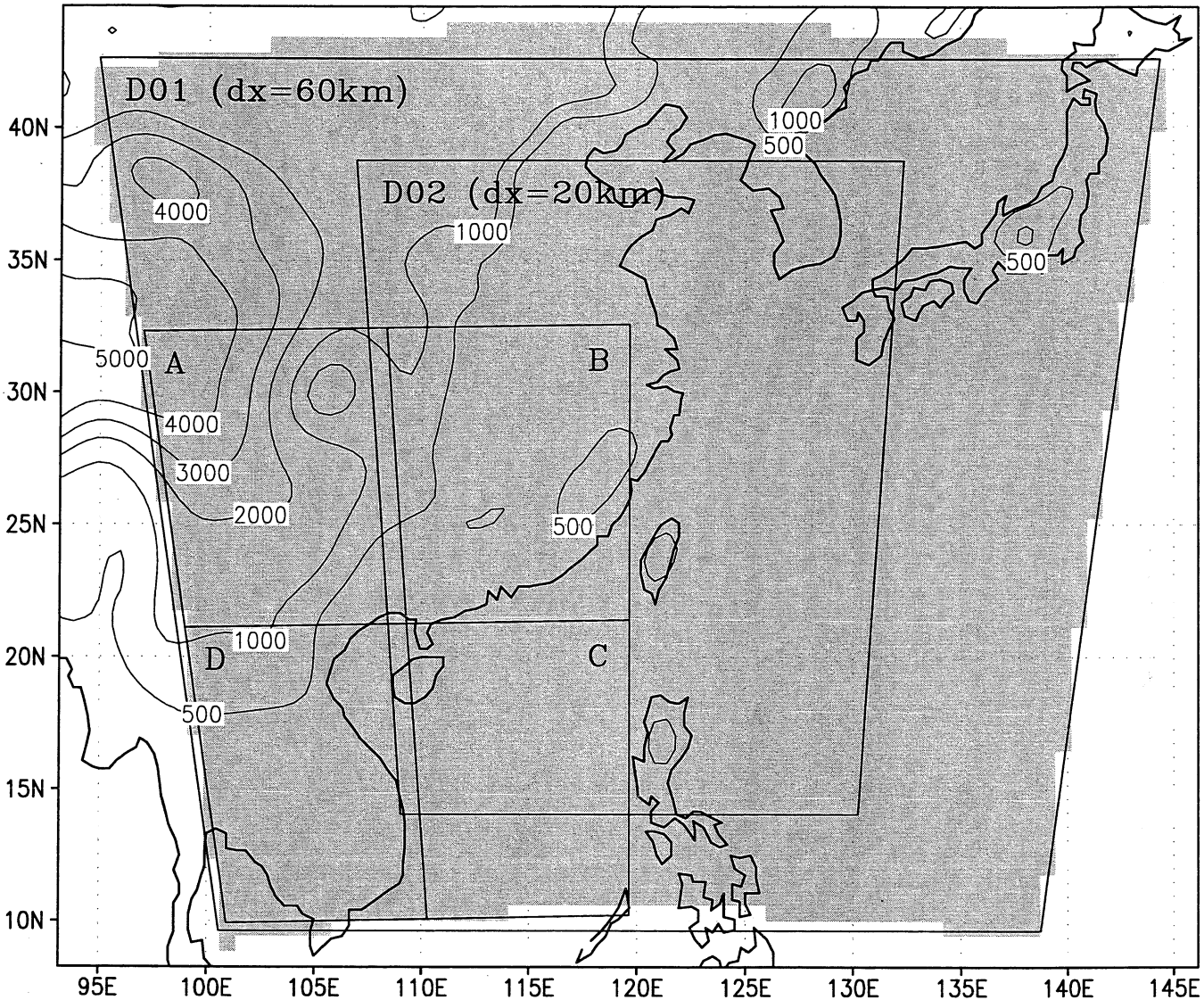

Fig.2 Model outer domain D01, inner domain D02, hydrology budget calculation domains A, B, C, and D, and topography (m).

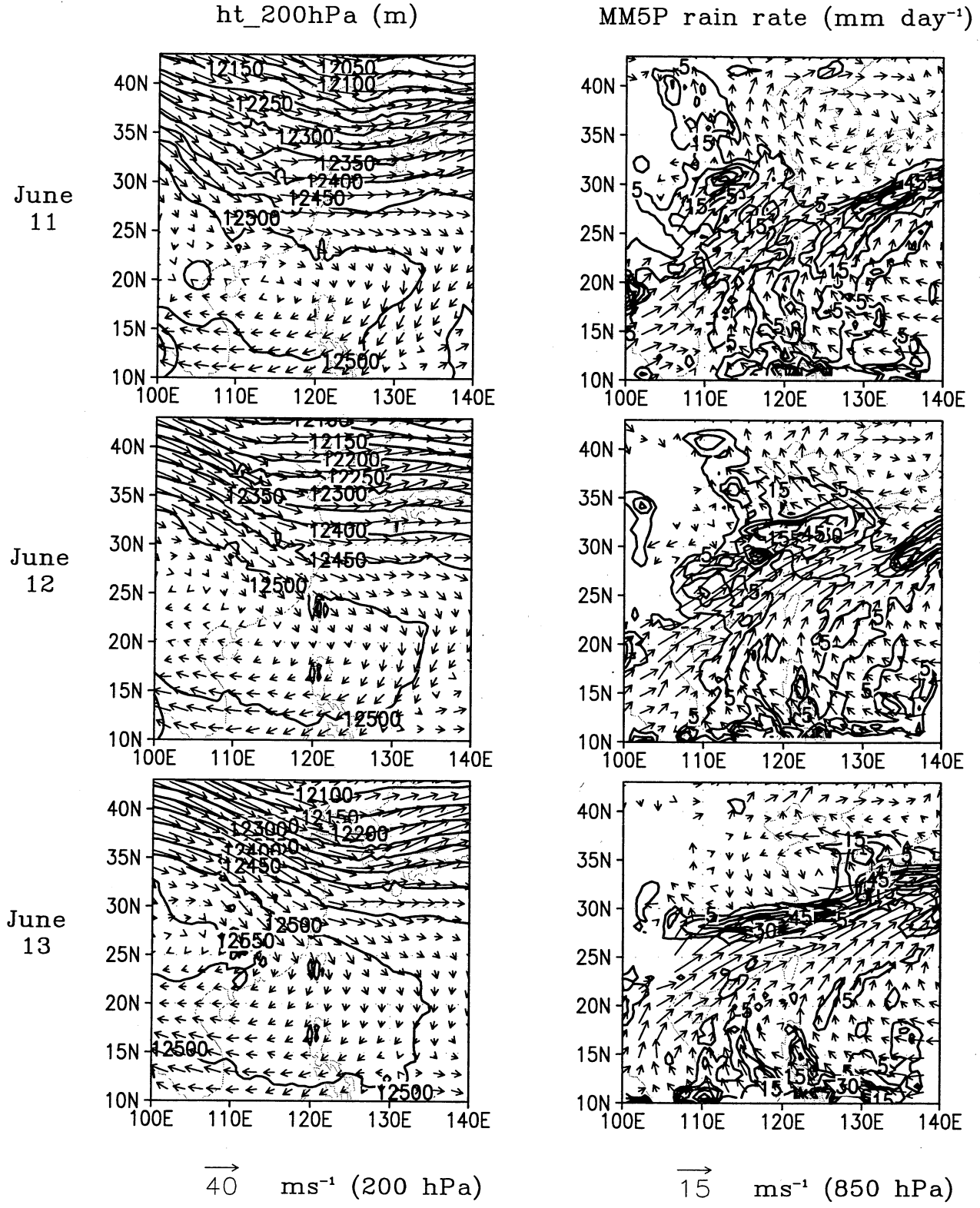
ht_200hPa (m)
MM5P rain rate (mm day⁻¹)
June 11
June 12
June 13
40N
35N
30N
25N
20N
15N
10N
100E
110E
120E
130E
140E
12150
12050
12100
12250
12300
12350
12400
12450
12500
12550
12600
12200
12750
40 ms⁻¹ (200 hPa)
15 ms⁻¹ (850 hPa)

Fig.3

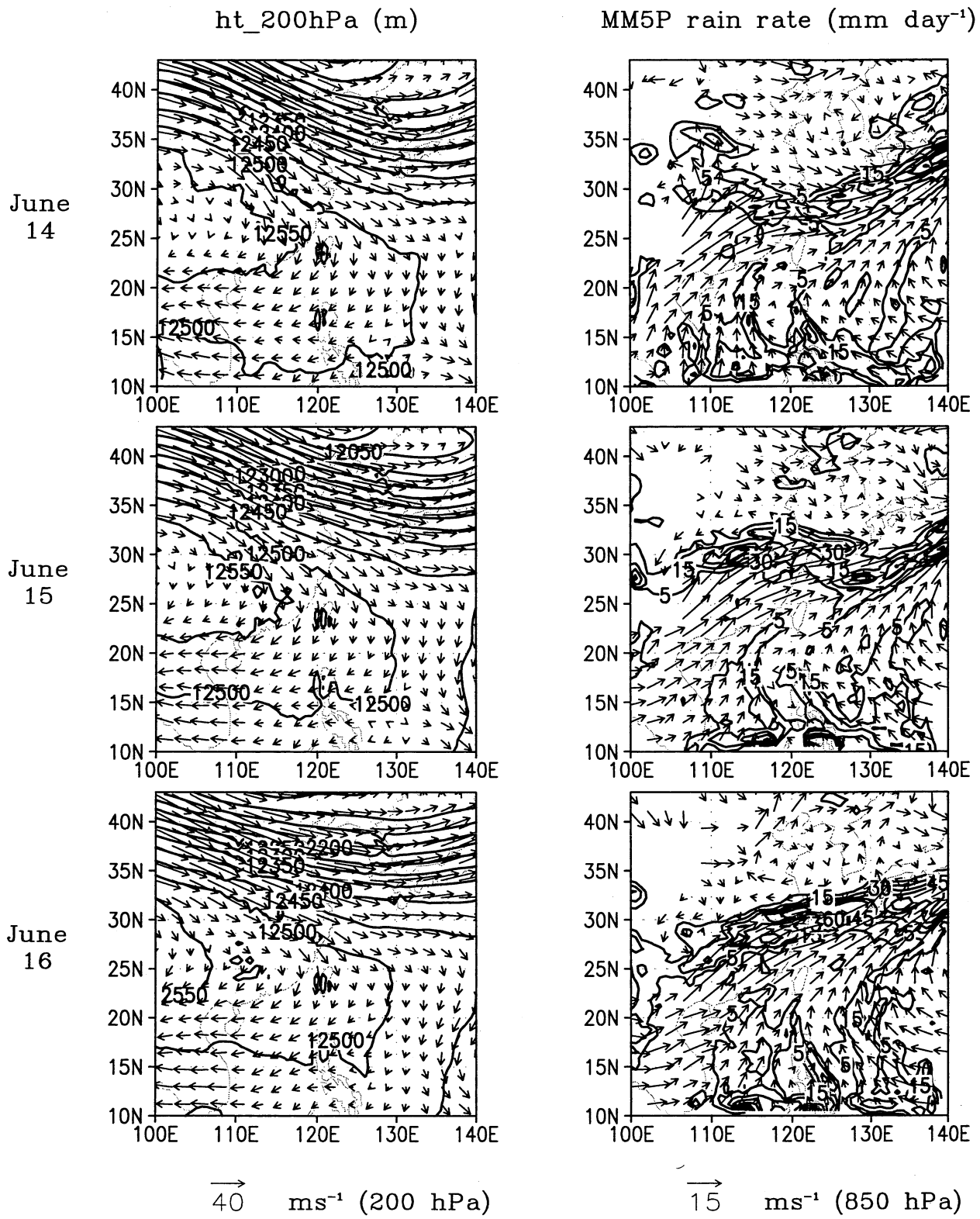

Fig.3 Height (m) and wind on 200hPa pressure surface (left panels), and daily rain rate (mm day^{-1}) and 850hPa wind (right panels), for control run CTRL, June 11–16, 1998.

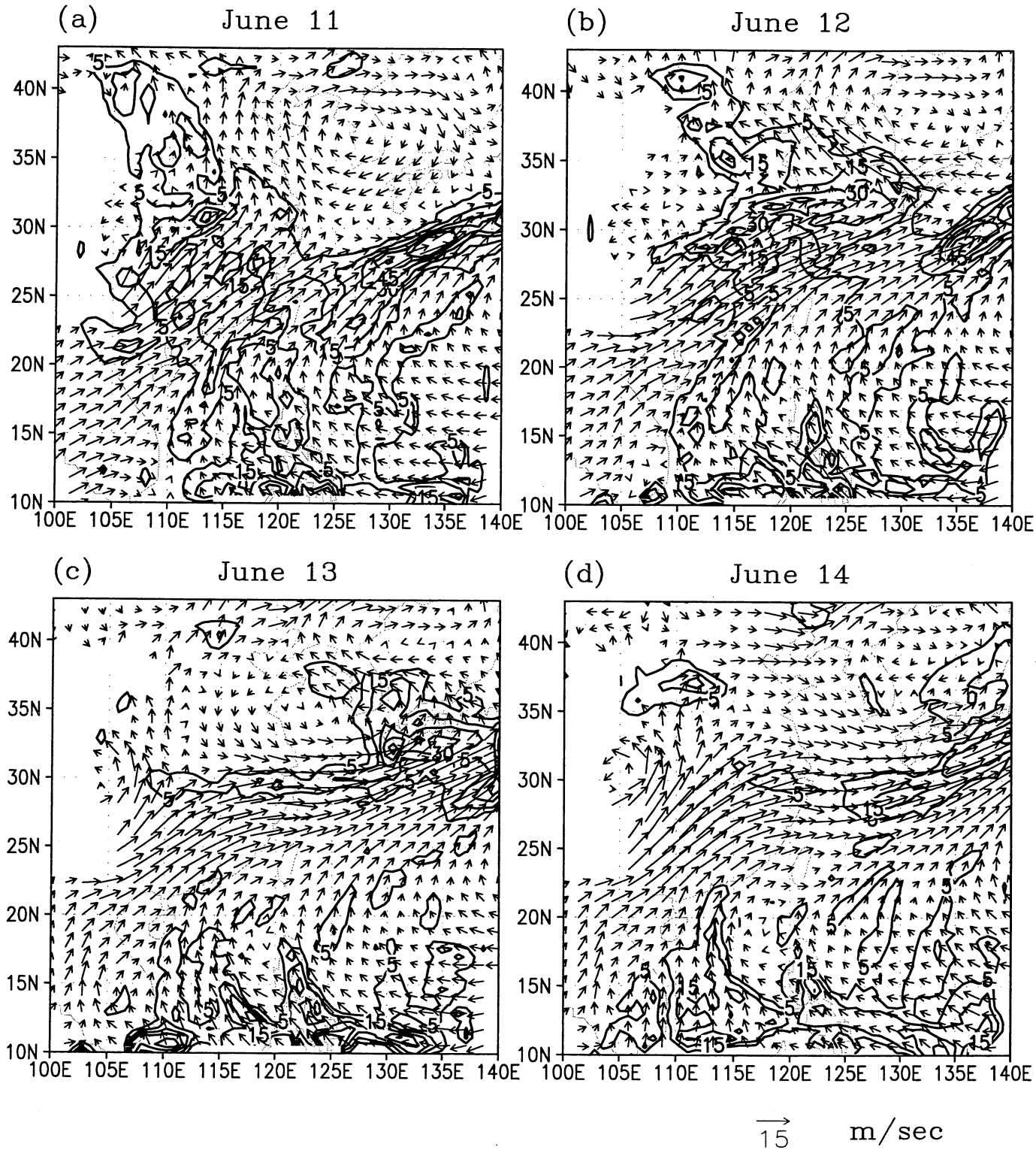

Fig.4 Daily rain rate (mm day^{-1}) and 850hPa wind for W50, June 11–14, 1998.

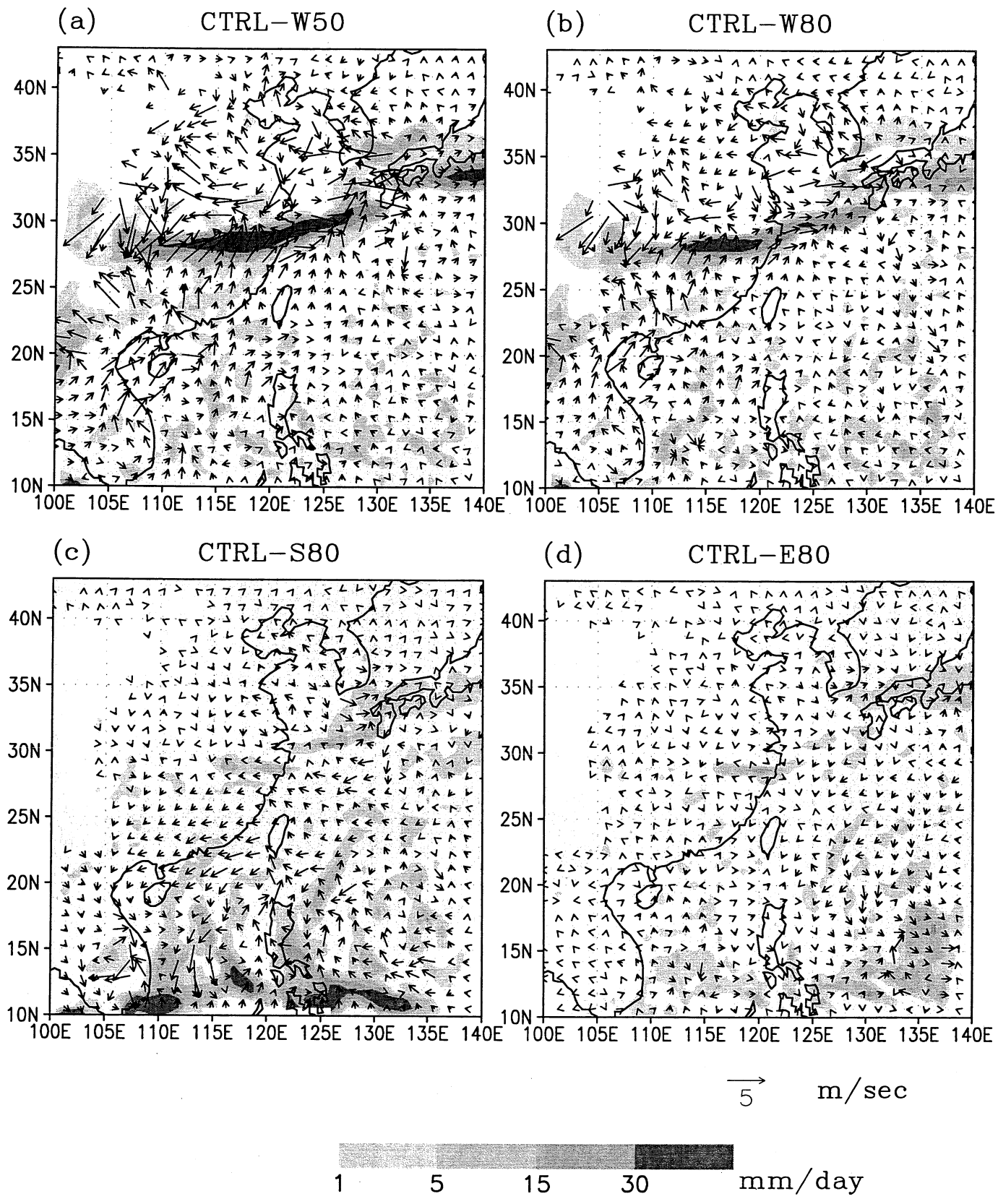

Fig.5 Differences of daily rain rate (mm day^{-1}) and 850hPa wind between control run and those with reduced moisture flux on one side of the outer boundary: (a) CTRL−W50, (b) CTRL−W80, (c) CTRL−S80, and (d) CTRL−E80, June 13, 1998.

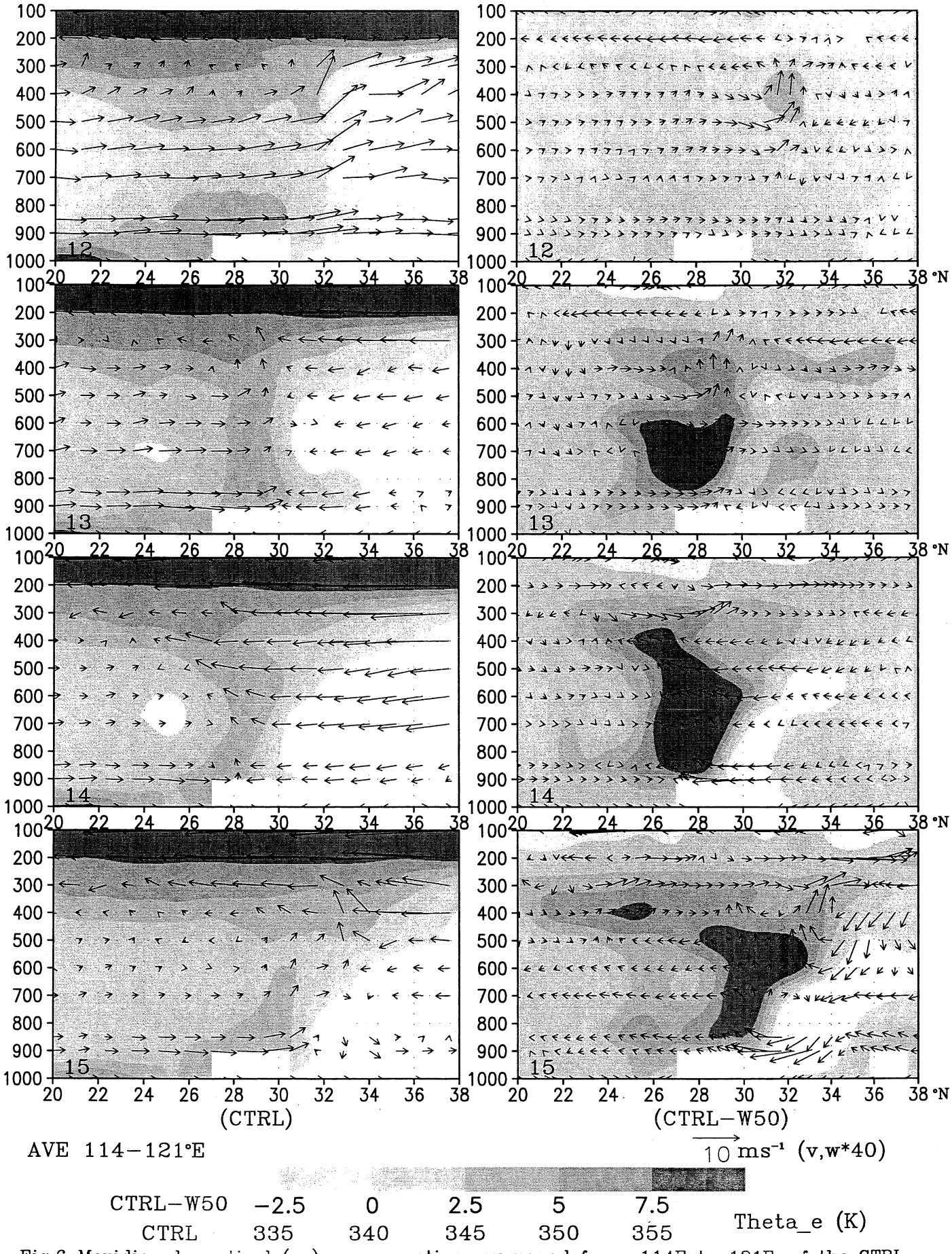

Fig.6 Meridional–vertical (yz) cross section, averaged from 114E to 121E, of the CTRL equivalent potential temperature and (v,w) wind (left panels), and their differences with W50 (right panels), June 12–15,1998.

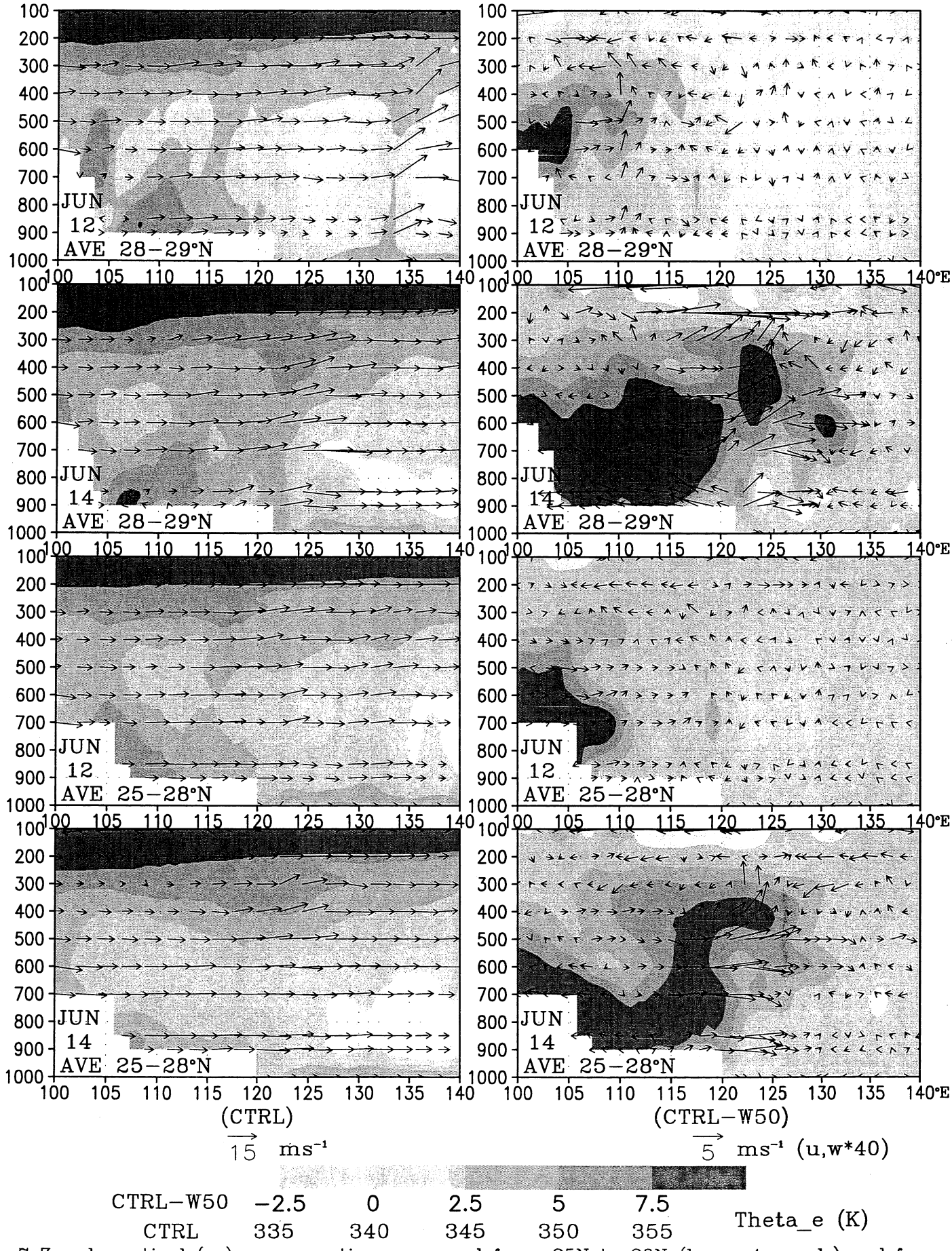

Fig.7 Zonal–vertical (xz) cross section, averaged from 25N to 28N (lower 4 panels) and from 28N to 29N (upper 4 panels), of the CTRL equivalent potential temperature and (u,w) wind (left panels), and their differences with W50 (right panels), June 12 and 14, 1998.

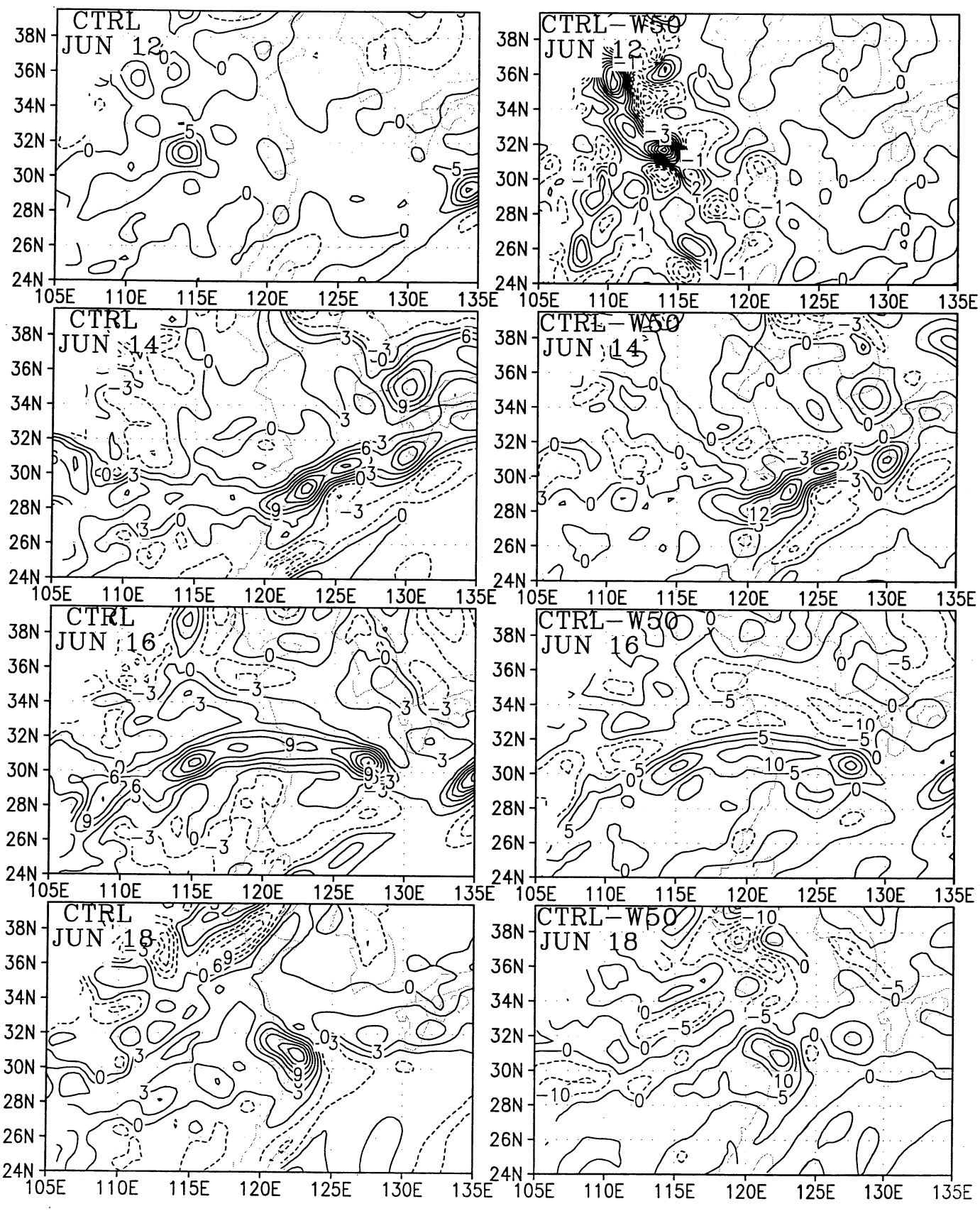

Fig.8 Vertical relative vorticity in CTRL, and its difference with that in W50 (CTRL-W50), at 00UTC June 12, 14, 16 and 18, 1998.

Water budget over domains A, B, C, and D (unit: 10E6 Kg/sec)

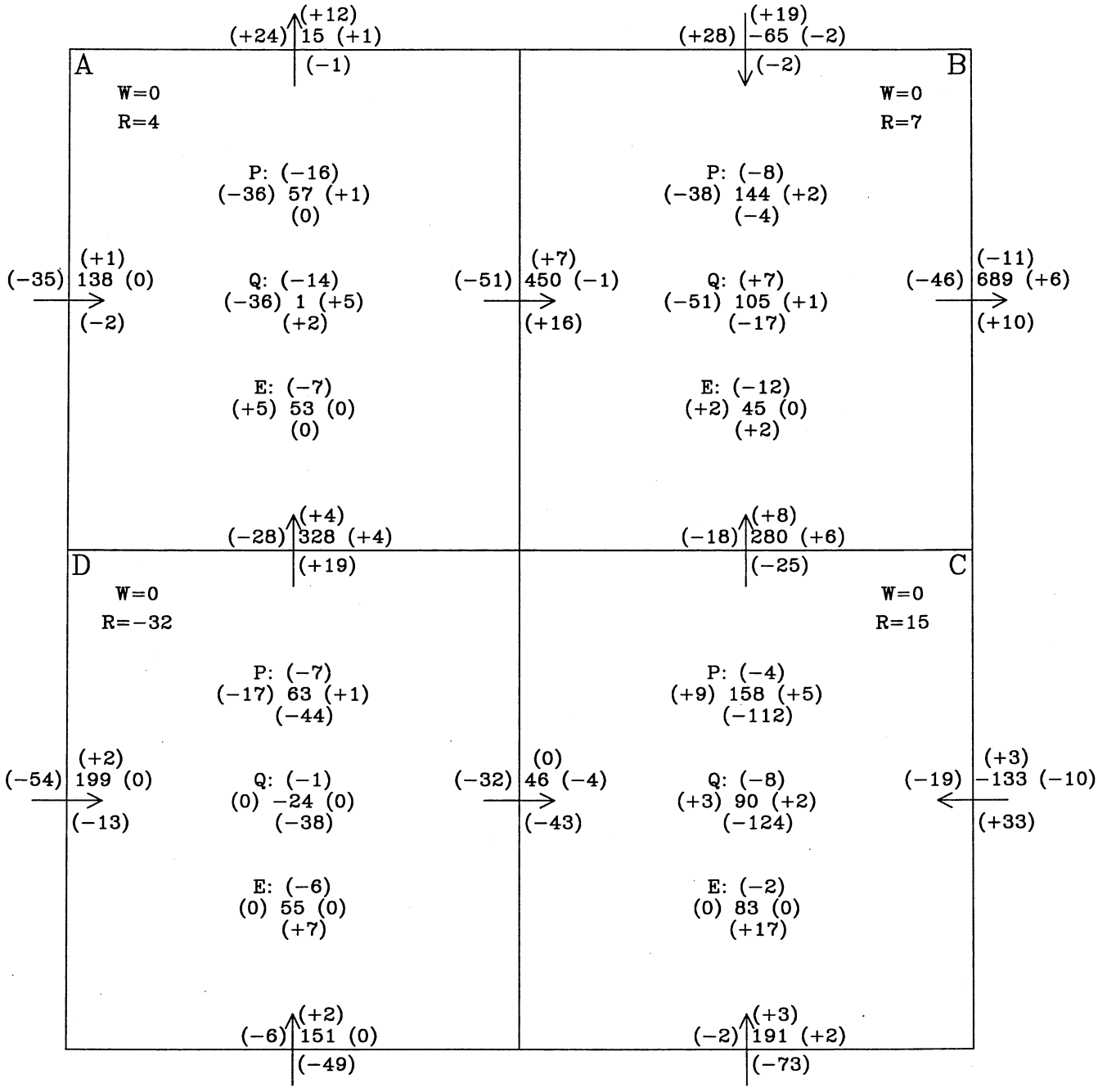

(NF−CTRL)
(W80−CTRL) CTRL (E80−CTRL)
(S80−CTRL)

Fig.9 Water budgets in domain A, B, C, and D (defined in Fig. 2), representing western China, Yangtze River Valey and southern China, South China Sea, and Indo−China Peninsula, respectively. Budget components P, E, Q, W and R are defined in Eq.(1). The unit is 10^6 Kg sec^{-1}.

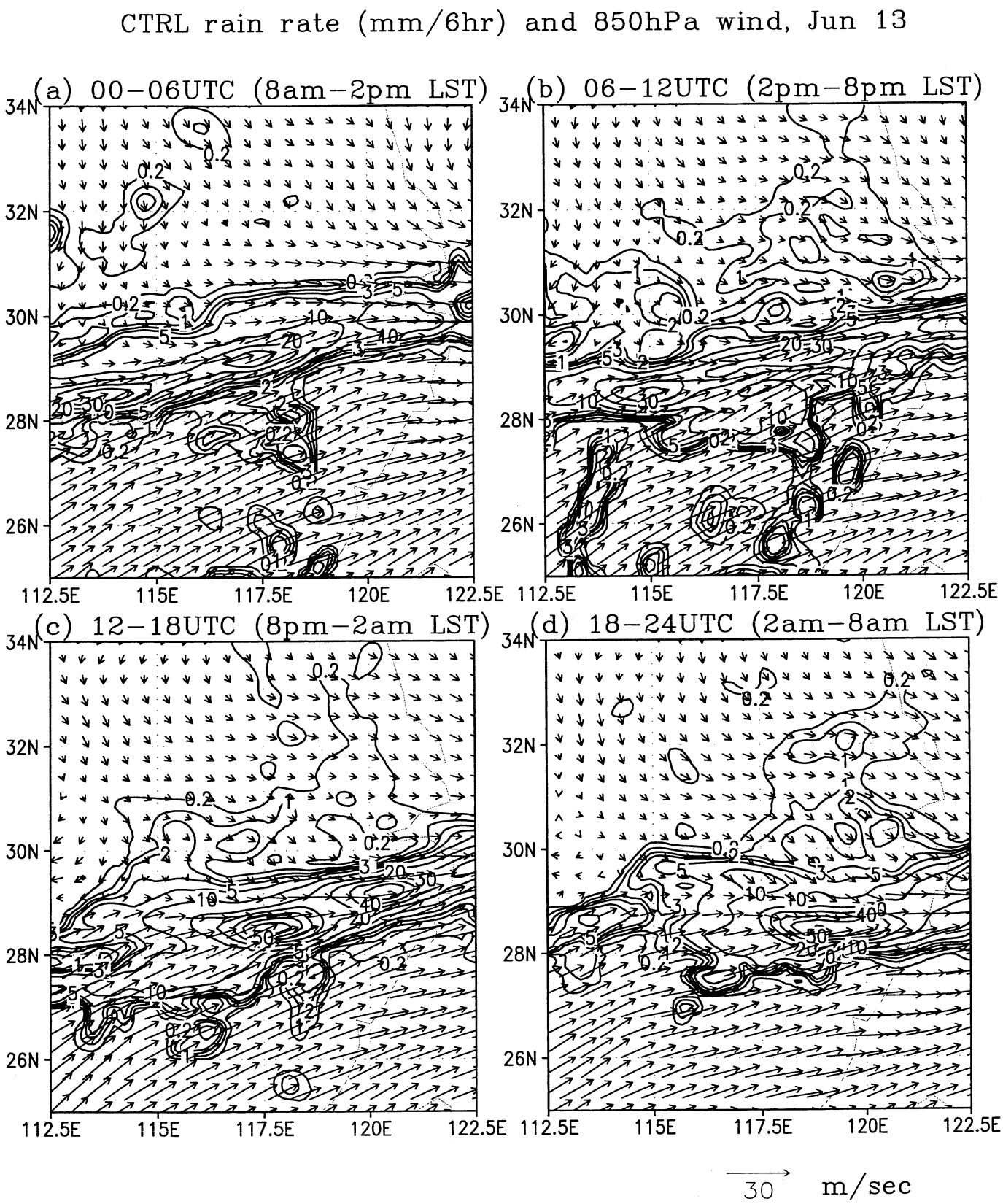

Fig.10 CTRL 6-hour rain rate and 850hPa wind on June 13, 1998. The times in the brackets are the local standard times (LST) corresponding to the UTC ones.

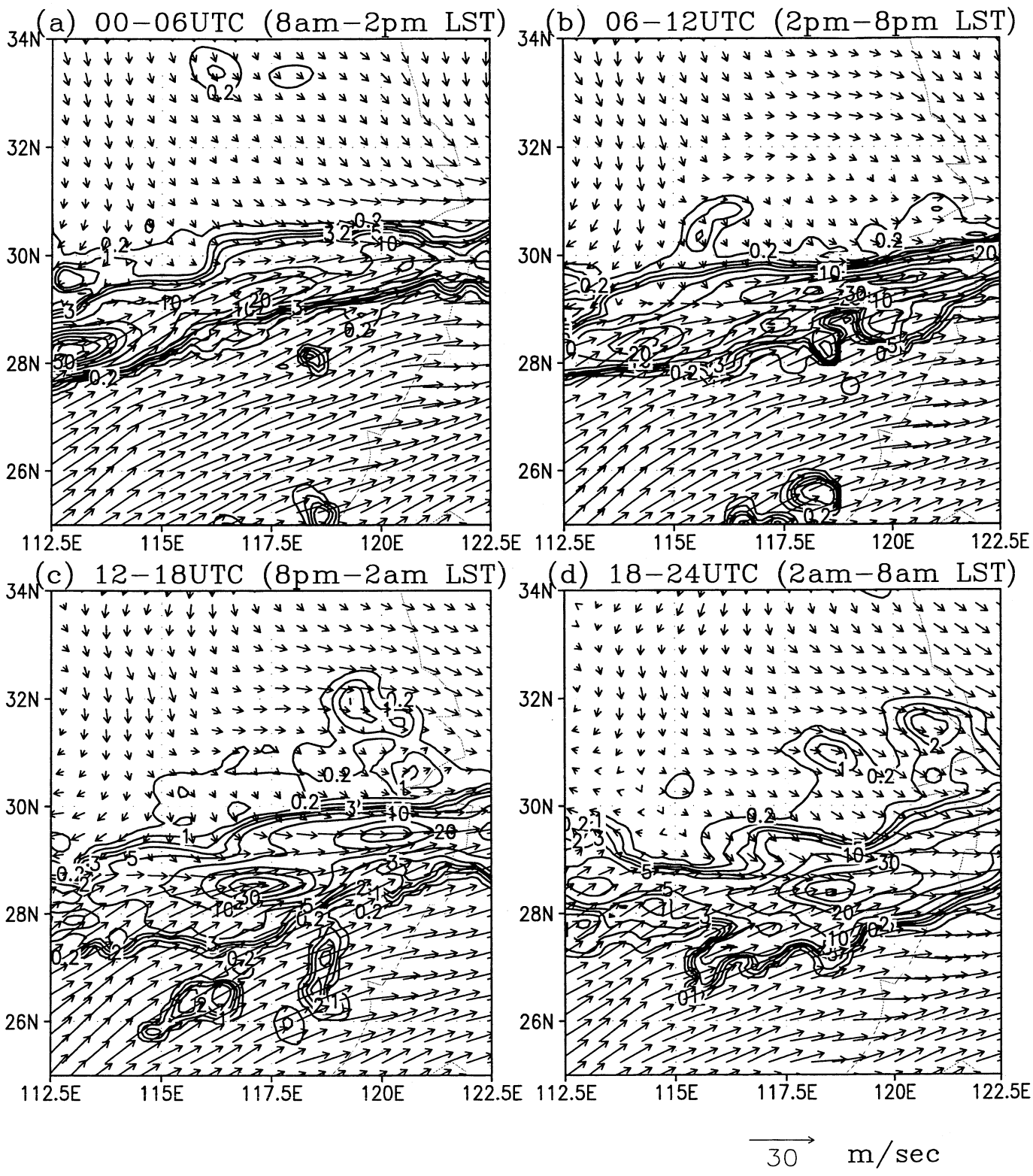

Fig.11 Same as Fig.10, except for NF, the run without precipitation-surface evaporation interaction.

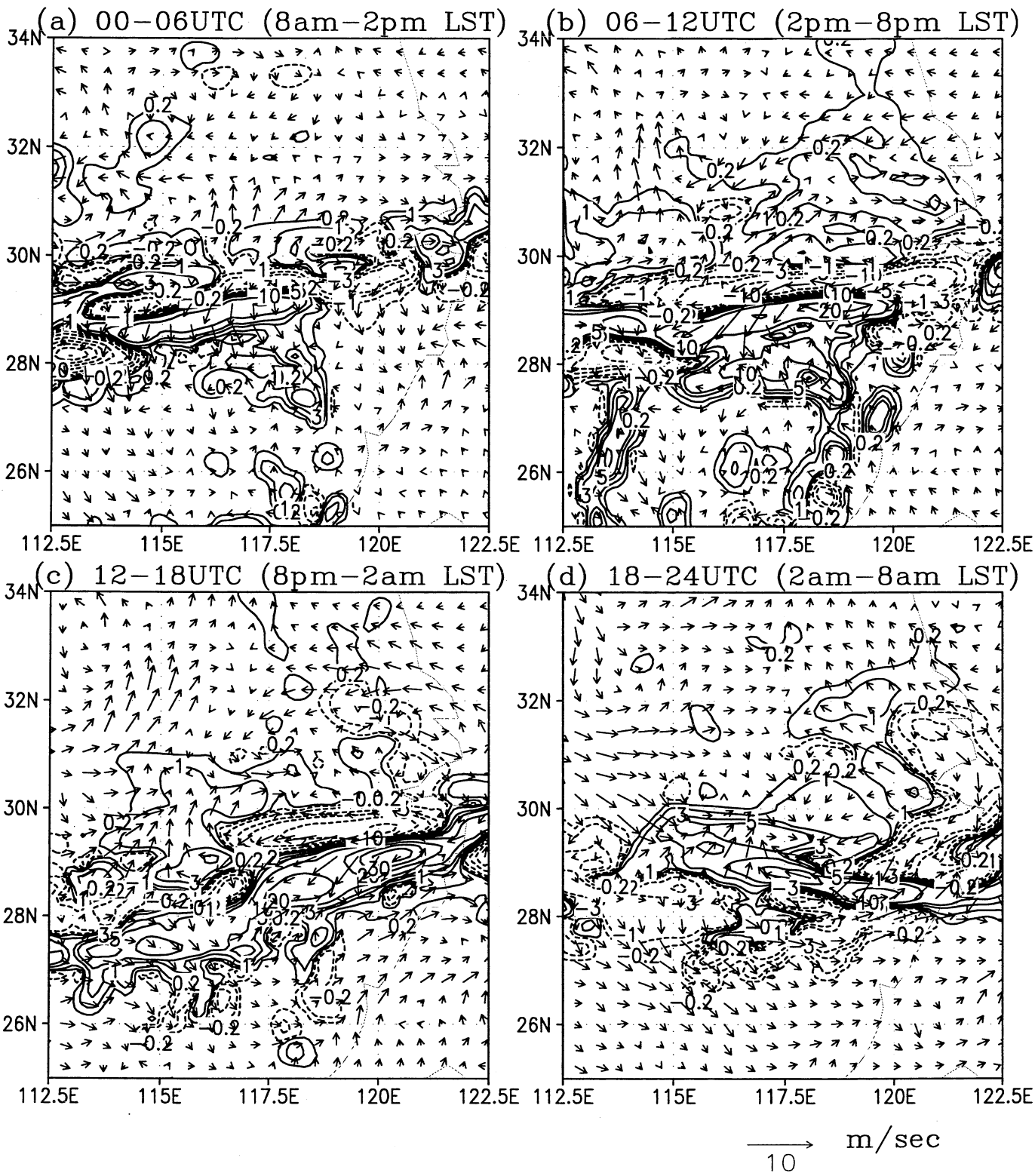

Fig.12 Difference between Fig.11 and 12 (CTRL−W50).

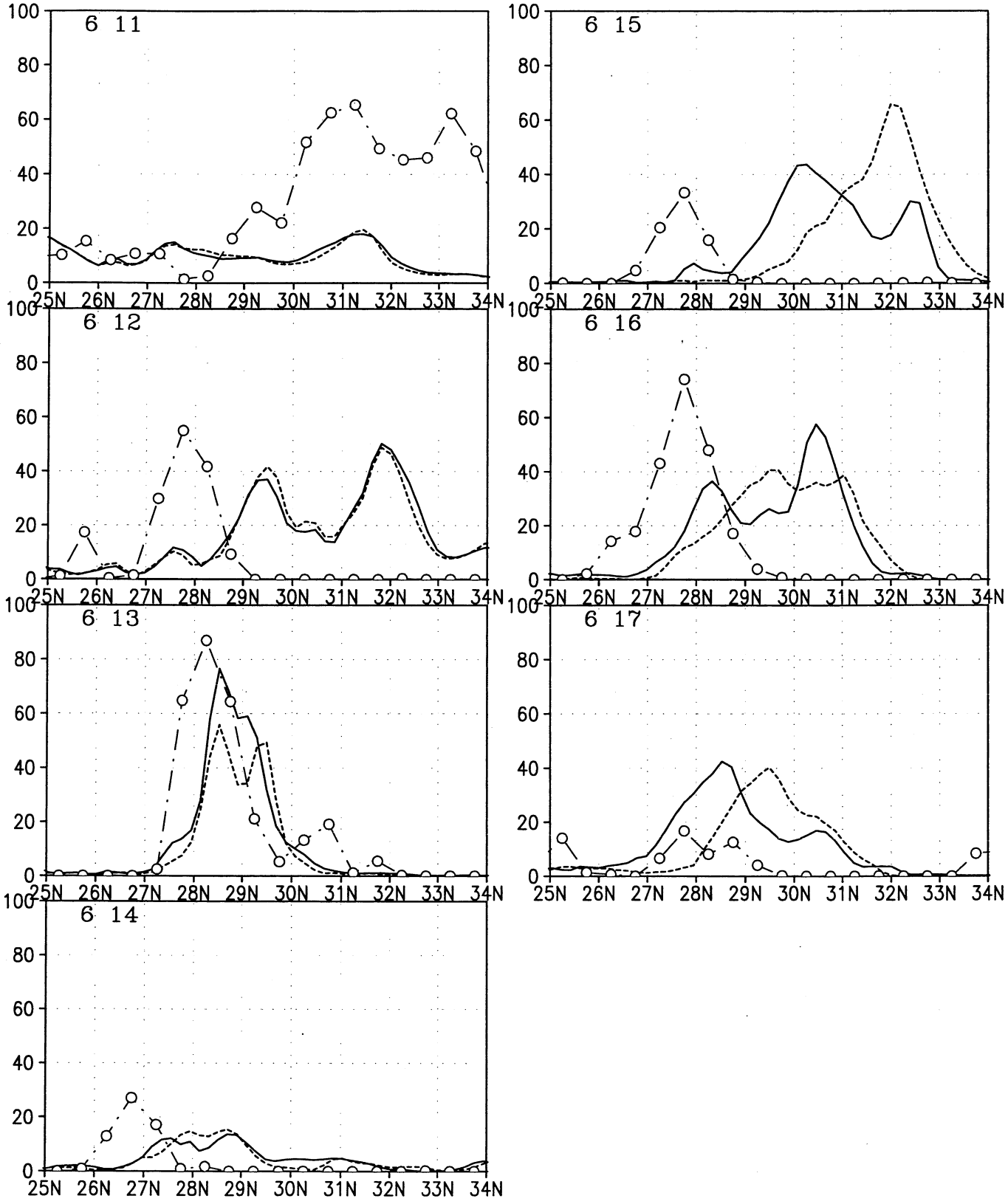

Fig.13 Meridional distribution of daily rain rate (mm day^{-1}), averaged from 114E to 121E: observation (dot-dash-circle), CTRL (solid), and NF (dash).

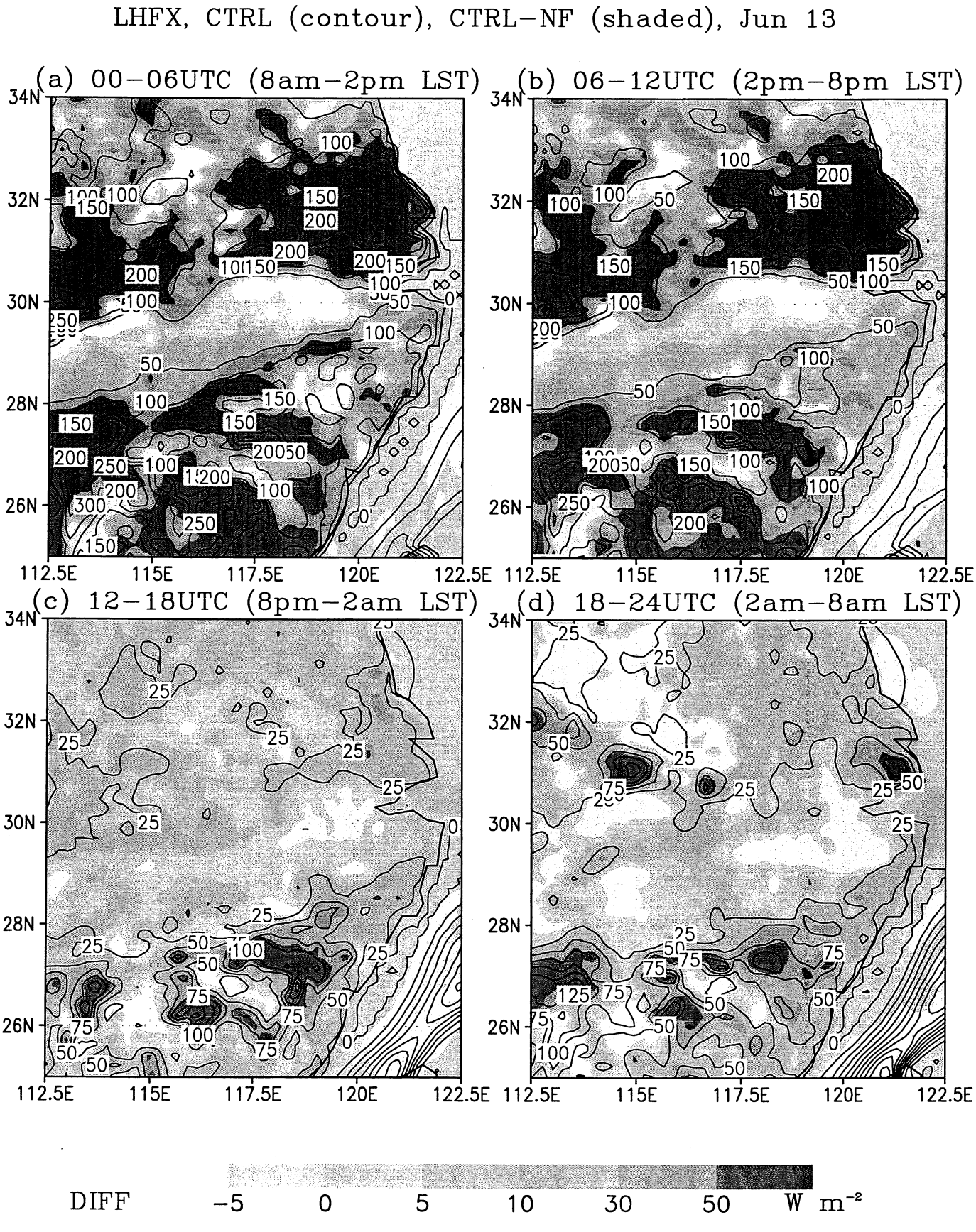

Fig.14 Surface latent heat flux (W m^{-2}) for CTRL (contoured), and the difference between CTRL and W50 (shaded), for the four quarters of June 13, 1998.

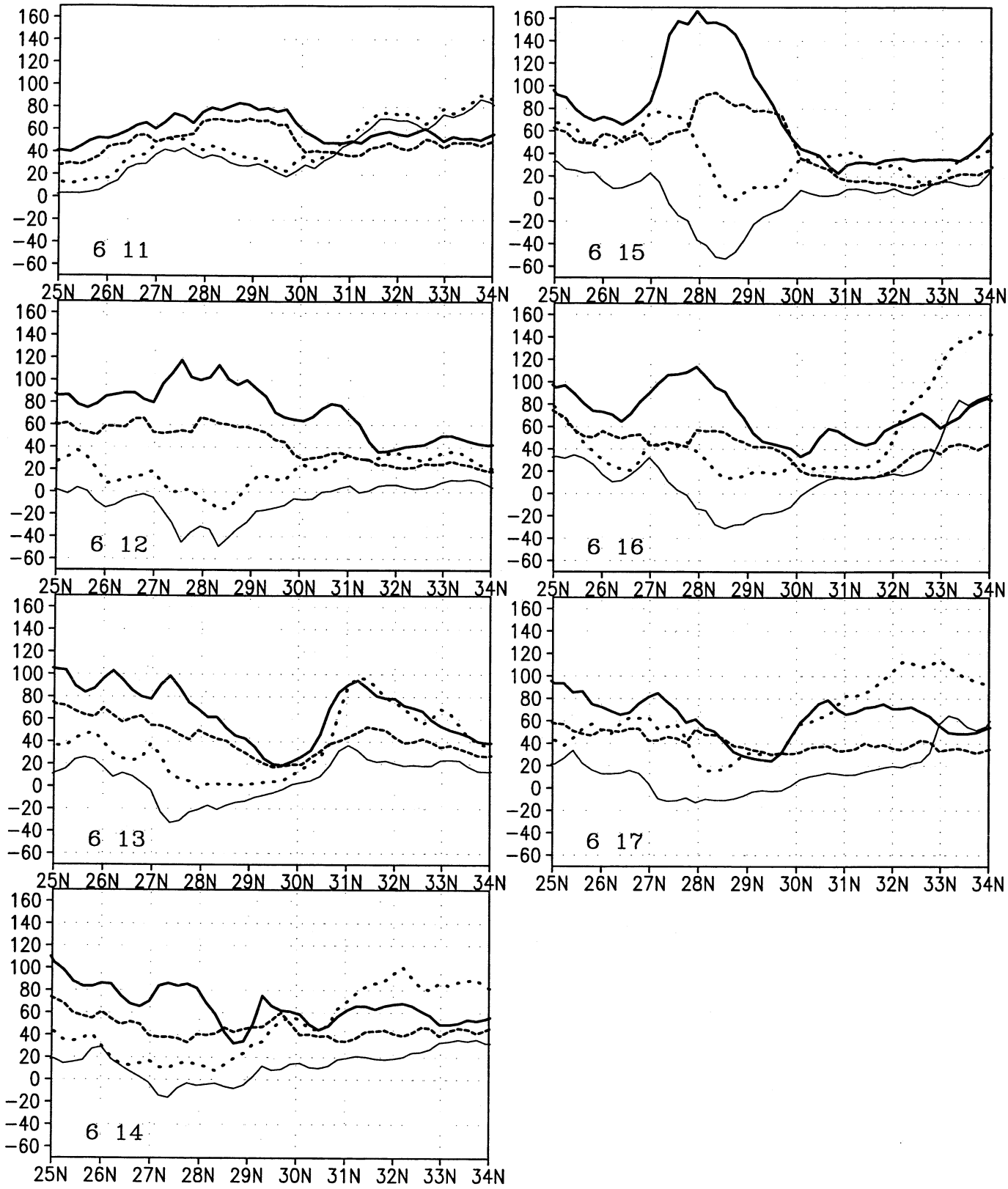

Fig.15 Meridional distribution of the surface sensible (SHFX) and latent (LHFX) heat fluxes (W m^{-2}), averaged from 114E to 121E: CTRL LHFX (thick solid), NF LHFX (dash), CTRL SHFX (thin solid), and NF SHFX (dot).

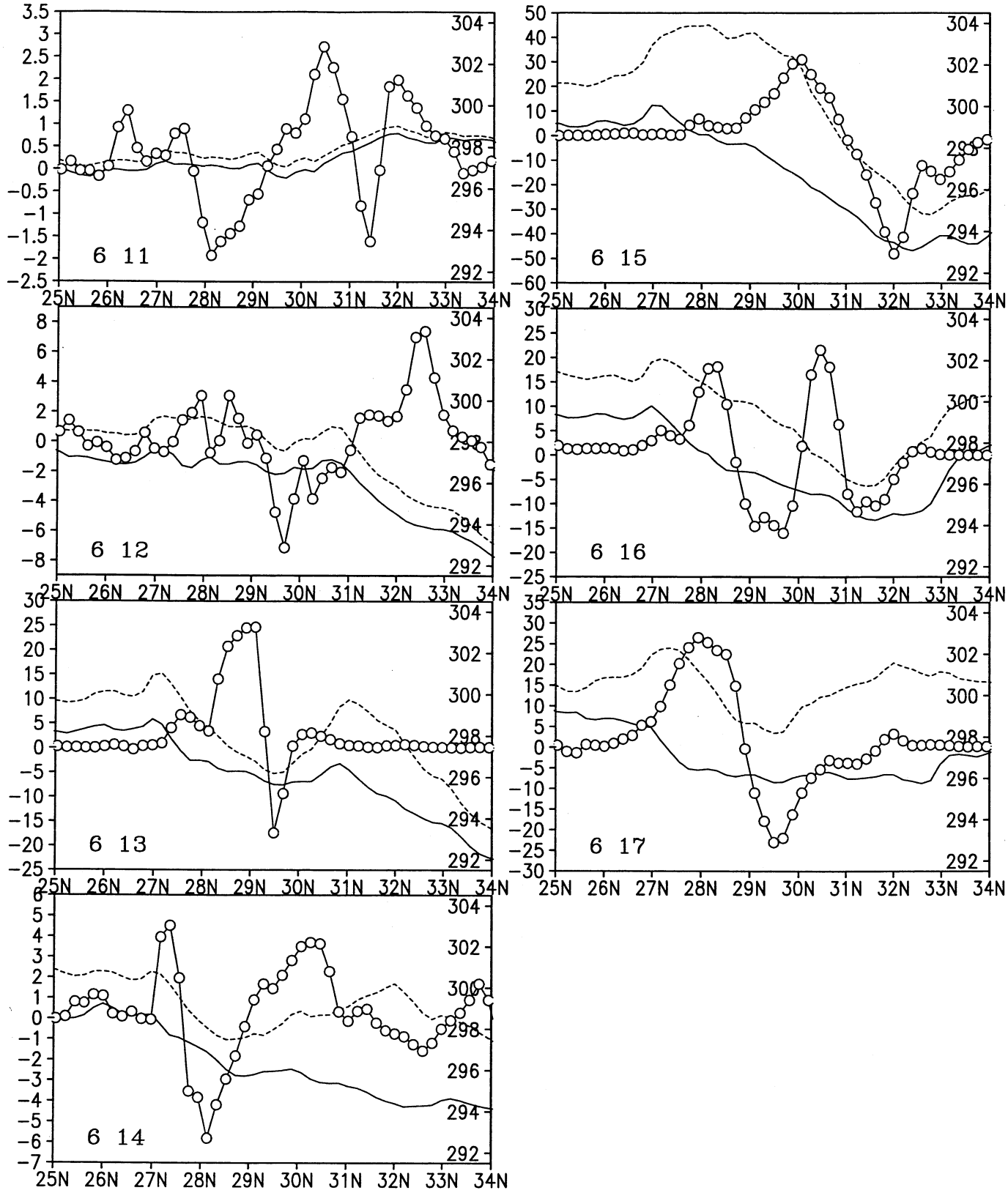

Fig.16 Meridional distribution of ground temperature (K) for CTRL (solid) and NF (dash), and the difference of daily rain rate between CTRL and NF (mm day^{-1}, circle), averaged from 114E to 121E.

Mechanisms of Torrential Rain Associated with the Mei-yu Development during SCSMEX-1998

by

Jian-Hua Qian, W.-K. Tao, and W. K.-M. Lau

Submitted to the *Monthly Weather Review*

Popular Summary

A case of torrential rainfall associated with the Mei-yu front, a nearly-stationary east-west frontal system that often persists in the spring from the east coast of China across Taiwan into the Pacific, is studied using an atmospheric weather model, the Penn State University/NCAR MM5, and a land-surface model, the NASA/GSFC PLACE (Parameterization for Land-Atmosphere-Cloud Exchange), that have been linked together. The influence of both remote and local sources of water vapor on the location and intensity of Mei-yu rainfall are studied by numerical experiments.

For this case, the results indicate that the source of water vapor for the heavy rainfall that occurred over the Yangtze river basin was the Bay of Bengal. The moisture was transported out of the southwest by strong low-level winds known as a low-level jet (LLJ). The storms responsible for the rainfall are themselves critical to the development and maintenance of the front. The heat released by the storms acts to increase the wind speed of the LLJ, providing a positive feedback that sustains the storm system along the Mei-yu front. It is found that local precipitation recycling shifts heavy rain toward the warm side of the front. The shift is due to the pronounced increase of atmospheric moisture and decrease of surface temperature on the warm side of the front.